NTNU

Norwegian University of
Science and Technology

CeO_2-ZrO_2-WO_3-based catalysts for Selective Catalytic Reduction of Nitrogen Oxides by Ammonia

Chun Kin Hui

Chemical Engineering
Submission date: June 2018
Supervisor: Magnus Rønning, IKP
Co-supervisor: Ole Håvik Bjørkedal, IKP

Norwegian University of Science and Technology
Department of Chemical Engineering

”The only true wisdom is in knowing you know nothing” - Socrates

Abstract

Cerium, zirconium and tungsten based catalysts with addition of 3% copper were prepared through the hydrothermal method and incipient wetness impregnation method. The three catalysts produced were named CZW (hydrothermal method), CZW-Cu (hydrothermal method) and CZW-CuImpr (3% Cu impregnated on CZW-support).

The pore structure, thermal stability, surface properties and compositions of the catalysts were characterized by XRD, XRF, BET, TGA, TPR, SEM and EDS. Activity test of the catalysts were performed in quartz capillary glass reactor connected to a mass spectrometer. The NO conversion for the catalysts were tested in the temperature range of 150-250 °C and correlated with a NO calibration of the mass spectrometer.

The catalyst synthesized through the hydrothermal method with the addition of 3% Cu was found to exhibit the highest NO conversion of 79.3% at 200 °C, but also indicated activity over the entire temperature range. The higher catalytic activity was attributed to the addition of small amount of Cu, which enhanced the SCR reaction. The hydrothermal synthesis method was concluded to be the better synthesis method for catalytic activity.

Sammendrag

Cerium-, zirkonium- og wolfram-baserte katalysatorer med tilsetning av 3% kobber ble preparert gjennom den hydrotermiske syntesen og impregnering. De tre katalysatorene ble kalt CZW (hydrotermisk metode), CZW-Cu (hydrotermal metode) og CZW-CuImpr (3% Cu impregnert på CZW-support).

Porestrukturen, termisk stabilitet, overflateegenskaper og sammensetningen av ble karakterisert ved hjelp av XRD, XRF, BET, TGA, TPR, SEM og EDS. Aktivitetstest av katalysatorene ble utført i kapillærglassreaktor koblet til et massespektrometer. NO-konvertering for katalysatorene ble testet i temperaturområ det 150-250C og korrelert med NO-kalibreringen av massespektrometeret.

Katalysatoren syntetisert gjennom den hydrotermiske metoden med tilsetning av 3% Cu var funnet til å ha den høyeste NO-konvertering på 79,3% ved $200\,^{\circ}\mathrm{C}$, men indikerte også tilsvarende aktivitet over hele temperaturområdet. Den høyere katalytiske aktiviteten til CZW-CuImpr var grunnet tilsetningen av den lille mengden Cu, som forbedret SCR-reaksjonen. Den hydrotermiske syntesemetoden ble konkludert med å være den bedre syntesemetoden for selektiv katalytisk reduksjons aktivitet.

Preface

I would like to thank my supervisor, Professor Magnus Rønning, for his guidance and help during the work on this thesis. I would also like to thank my co-supervisor Ole Håvik Bjørkedal for his help and guidance with experimental methods, data interpretation and feedback.

Thanks to Karin Wiggen Dragsten for her training and assistance in experimental apparatus, and the staff at NTNU Nanolab for their training and help.

I declare that this is an independent work according to the exam regulations of the Norwegian University of Science and Technology.

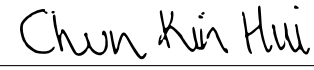

Chun Kin Hui June 21, 2018, Trondheim

Table of Contents

List of Tables

List of Figures

Abbreviations

Abbreviation	Description
a.u.	Arbitrary unit
BET	Brunauer, Emmett and Teller
BJH	Barrett, Joyner, Halenda
CXA	Computer-assisted X-ray analyzer
CZW	Selected notation for Ce, Zr and W catalyst
CZW-Cu	Selected notation for Ce, Zr, W and Cu catalyst
CZW-CuImpr	Selected notation for Ce, Zr, W with impregnated Cu catalyst
DSC	Differential Scanning Calorimetry
EDS	EnergyDispersive X-ray Spectroscopy
EDX	Energy Dispersive X-ray
EDXRF	Energy Dispersive system (XRD)
FET	Field Effect Transistor
i.e.	id est (latin) - that is
IMO	International Maritime Organization
IUPAC	International Union of Pure and Applied Chemistry
LNG	Liquefied Natural Gas
MCA	Multichannel analyzer
MFC	Mass Flow Controller
MS	Mass spectroscopy
NO_x	Nitrous Oxides
ppm	parts per million
SCR	Selective Catalytic Reduction
SEM	Scanning Electron Microscopy
SO_x	Sulfuric Oxides
STA	Simultaneous Thermal Analysis
S(T)EM	Scanning (Transmission) Electron Microscopy
TCD	Thermal Conductivity Detector
TEM	Transmission Electron Microscopy
TG	Thermogravimetric
TGA	Thermogravimetric Analysis
TPD	Temperature Programmed Desorption
TPO	Temperature Programmed Oxidation
TPR	Temperature Programmed Reduction
WDXRF	Wavelength Dispersive systems (XRF)
XRD	X-Ray Diffraction
XRF	X-Ray Fluorescence

List of symbols

Symbol	Dimension	Description
A	m^2/g	Total surface area
A	-	Ampere
A_0	$m^2/molecule$	Area each molecule occupies (N_2)
Å	-	Angstrom
d	Å	Lattice plane distance
$< L >$	nm	Crystal diameter
N_0	-	Number of molecules adsorbed in the first monolayer
r	cm	pore Radius
R	$JK^{-1}mol^{-1}$	Universal gas constant
P	mmHg	Pressure
P_0	mmHg	Equilibrium pressure
V_a	cm^3	Total adsorbed gas volume
V_0	cm^3	Volume adsorbed in the first monolayer
$\bar{V}$	cm^3	Molar Volume
n	-	Order of reflection in Bragg's law
α	cm^{-3}	Slope of BET isotherm linear plot
η	cm^{-3}	Intercept of BET isotherm linear plot
λ	Å	Wavelength
σ	Nm^-1	Surface tension
θ	-	Angle
χ	-	Ratio of desorption rate constant for second and first BET monolayer

Chapter 1

Introduction

The marine transportation sector has traditionally used heavy fuel oil as its primary energy source. However, due to increased emission regulations adopted by the International Maritime Organization (IMO) [1] the search for an alternative low sulphur content fuel was pursued. The motivation behind the more stringent regulation was linked to the harmful effects on the environment and human health, such as acid rain and respiratory diseases [2]. Which in turn is related to the emission of sulphur dioxide (SO_2) and particulate matter released by heavy fuel oil.

With the increased availability and production of natural gas in North-America [3], liquefied natural gas (LNG) has been considered as a reasonable alternative to heavy fuel oil. Advantages such as lower pollution of sulphur, nitrogen oxides (NO_x) and more efficient engines makes LNG a promising substitution. Increased engine efficiency through energy efficiency (less heat loss) leads to a lower exhaust temperature. State-of-the-art NO_x removal from heavy duty engine exhaust includes Selective Catalytic Reduction (SCR) where NO_x is reduced by a reducing agent such as ammonia (NH_3). Nowadays, the most known NH_3-SCR catalyst is $V_2O_5-WO_3/TiO_2$, but due to the narrow working temperature window ($300-400\,^{\circ}C$)[4], the toxicity of vanadium species and the formation of N_2O at higher temperature it is expected to have reduced efficiency in the modern engines. Consequently, efforts have been made to create an environmentally-friendly and highly efficient SCR catalyst at a lower and wider temperature range.

The goal of this project is to develop $CeO_2-ZrO_2-WO_3$ based catalysts suited for the low-temperature NH_3-SCR, based on a synthesis procedure reported by Song et al. [5, 6]. Different characterization techniques are used to determine catalyst properties, such as thermal stability, pore size, chemical composition, crystallinity and surface area. The catalysts are also tested in a capillary reactor connected to a mass spectrometer to determine their activity.

1.1 Background

Nitrogen oxides emitted from transportation is considered as a serious threat to both the environment and human health [7]. The effects of NO_x includes acid rain, formation of surface ozone and direct effects on the human health. Where the effects on human health includes decreased lung function, increased risk of respiratory conditions and increased response to allergens. NO_x also contributes to the formation of fine particles and ground level ozone, which are associated with serious health issues.

NO_x is formed in several ways, but most commonly during combustion in flame. Where the main source of NO_x stems from thermal NO_x, which occurs at temperature above $1300\,^{\circ}\mathrm{C}$ [8]. Other sources are fuel NO_x which comes from N-containing species in coal, biomass and oil. While prompt NO_x occurs at temperature below the limit of thermal NO_x. Some NO_x are also formed by the reaction between N_2 and O_2 in air at higher temperatures. Based on the impact on environment, human health and increasingly stringent emission regulations, it is imperative to reduce NO_x emissions.

The most widely used technology in reducing emissions of NO_x is the SCR [9, 10], where NO_x is reduced to N_2 by using NH_3 as the reductant. Due to the fact that NO_x in diesel exhaust mainly consists of NO ($> 90\%$), the main reaction behind the NH_3-SCR is:

$$4\,\mathrm{NO} + 4\,\mathrm{NH_3} + \mathrm{O_2} \longrightarrow 4\mathrm{N_2} + 6\,\mathrm{H_2O} \tag{1.1}$$

The reaction consuming no oxygen is much slower and therefore not as relevant in lean exhaust:

$$4\,\mathrm{NH_3} + 6\,\mathrm{NO} \longrightarrow 5\mathrm{N_2} + 6\,\mathrm{H_2O} \tag{1.2}$$

On the contrary, the reaction rate with equimolar amounts of NO and NO_2 is much faster compared to Equation 1.1 [11]:

$$4\,\mathrm{NH_3} + 2\,\mathrm{NO} + 2\,\mathrm{NO_2} \longrightarrow 4\mathrm{N_2} + 6\,\mathrm{H_2O} \tag{1.3}$$

Any excess of NO_2 after Equation 1.3 can react in the following reaction:

$$6\,\mathrm{NO_2} + 8\,\mathrm{NH_3} \longrightarrow 7\mathrm{N_2} + 12\,\mathrm{H_2O} \tag{1.4}$$

Therefore, the conversion of NO to NO_2 in the oxidation reactor should not exceed 50%, as this will reduce the performance of the SCR catalyst [11].

The classic catalyst used in SCR is the vanadium oxide supported on titania (V_2O_5/TiO_2) catalyst, due to its high conversion of NO_x and the resistance towards sulphur poisoning,

as sulphur can deactivate the catalyst. Other alternative catalysts have been proposed as a possible substitution, such as $Fe_2O_3-Cr_2O_3-Cu$/alumina, noble metals and zeolites as structural promoter.

Chapter 2

Theory and literature

This section covers the theoretical background for the experimental method and analysis techniques used in this project. Section 2.1 explains the choice of catalyst material while section 2.2 contains the principles for the catalyst preparation via hydrothermal method and impregnation. Section 2.3 focuses on the fundamental theoretical principles for all characterization methods used.

2.1 Catalyst material

The commercial SCR catalyst are mainly V_2O_5/TiO_2 promoted by either MoO_3 or WO_3 [12, 13, 14], but some unavoidable problems still remain, such as the environmental toxicity of vanadium species, the narrow reaction temperature window (300-400 °C) and the formation of N_2O at high temperature [15]. Consequently, many kinds of non-vanadium catalysts with high catalytic activity have been tested for NH_3-SCR reaction. Noble metal-based catalysts are usually known for their excellent stability and activity, but their high cost and narrow temperature window impede their industrial application [16]. Zeolite-based Fe and Cu catalysts also showed promising property such as high NO_x removal efficiency, but despite this the susceptibility of sulfur poisoning and the poor hydrothermal stability are still the main obstacle [17, 18, 19].

Recently, cerium-based oxides with excellent redox property and high oxygen storage capacity have been widely used for NH_3-SCR reaction [20, 12]. However, pure CeO_2 faces problems due to inferior thermal stability and that the pore structure collapses at high temperatures, but by introducing ZrO_2 the thermal and structure stability of CeO_2 is noticeably promoted [21]. The $CeZrO_x$ solid solution is also considered as a promising materials for NOx removal [22]. WO_3 is a key component in the commercial SCR catalyst as catalyst promoter. Research on W-based catalyst has shown high activity towards NH_3-SCR reaction due to the improvement of surface acidity by promoting the adsorption NH_3 capacity [23]. Li et al.[24] reported that a WO_3/CeO_2-ZrO_2 catalyst showed a high catalytic activity at 300-500 °C prepared by impregnation method. However, due to increasingly stringent emission standards of diesel exhaust, these catalysts are also struggling to meet the standards, which spurred more research towards CeO_2-ZrO_2-WO_3-based catalysts. Ning et al. [4] prepared several CeO_2-ZrO_2-WO_3 catalysts by different methods. The most promising catalyst was prepared by hydrothermal method, where they reported a NO conversion of more than 90% obtained between 195-450 °C, indicating a promising catalyst to pursuit and develop.

Cu is widely used as active species in different catalytic processes, while also considered to be a possible substitution of noble metal catalysts in many cases [25]. Several studies reports that catalysts like ZrO_2 and CeO_2, when loaded with small amounts of Cu, enhances the selective catalytic reduction of NH_3 [26, 27, 25].

Based on the above-mentioned discussion this project focuses on synthesizing CeO_2-ZrO_2-WO_3 catalysts through the hydrothermal method. The same catalyst modified with Cu is also explored.

2.2 Hydrothermal synthesis

Various definitions of hydrothermal synthesis have been proposed by scientists in literature. In 1913, Morey and Niggli defined hydrothermal synthesis as ".. in the hydrothermal method the components are subjected to the action of water, at temperatures generally near though often considerably above the critical temperature of water ($370\,^{\circ}\mathrm{C}$) in closed bombs, and therefore, under the corresponding high pressures developed by such solutions" [28]. Rabenau in 1985 defined it as "Heterogeneous reaction in aqueous media above $100\,^{\circ}\mathrm{C}$ and 1 bar are usually referred to as a "hydrothermal synthesis" [29].

The principle behind hydrothermal synthesis is that an insoluble material at ambient temperatures can be made soluble using higher pressures and temperatures. The synthesis is a complex process consisting of three basic steps: The achievement of nucleation, supersaturation and crystal growth. The formation of crystalline entity from a solution begins with the nucleation process. By definition, nucleation is a series of atomic or molecular processes by which the molecules or atoms of a reactant phase rearrange into a cluster large enough to have the ability to grow irreversibly larger. Supersaturation is the driving force needed for the nucleation and is defined as the difference in chemical potential between a molecule in solution and that in the bulk of a crystal phase [30].

In general, the synthesis is carried out at $85-180\,^{\circ}\mathrm{C}$ under atmospheric or autogenous water pressure (0.5 - 1 MPa) with residence times of 1-6 days, where an autoclave is typically used as synthesis vessel. After synthesis, the product is separated either by centrifugation or filtration, washed, dried, and calcined [31].

2.2.1 Impregnation and drying

Impregnation is a common method used in catalyst preparation, where the purpose is to achieve stabilization of high/optimal dispersion of active component(s) against sintering, reduce cost and utilization of important mechanical and morphological properties of the support.

The method involves three steps, where the first step is contacting the support with the impregnating solution for a period of time. The second step is to remove the imbibed liquid through drying, and the third step is activating the catalyst through calcination, reduction or other treatments appropriate. Impregnation can be classified in two categories, based on the volume of solution added. These two are namely "incipient wetness impregnation (dry impregnation)" and "wet impregnation".

The simplest method to carry out impregnation is by contacting a previously dried support with a known pore volume, with a volume of solution equal to the known pore volume containing the precursor of the active phase. The solution is then drawn into the pores

by capillary suction, as illustrated in Figure 2.1. Proper wetting is when no excess of solution remains outside the pore space. This procedure is also called incipient wetness or dry impregnation. Another method of impregnation can be carried out in diffusional conditions, by immersing a water filled support in the precursor solution, also called wet impregnation. This method should be avoided when the interaction between the support and precursor is too weak to guarantee deposition of the precursor [32, 33].

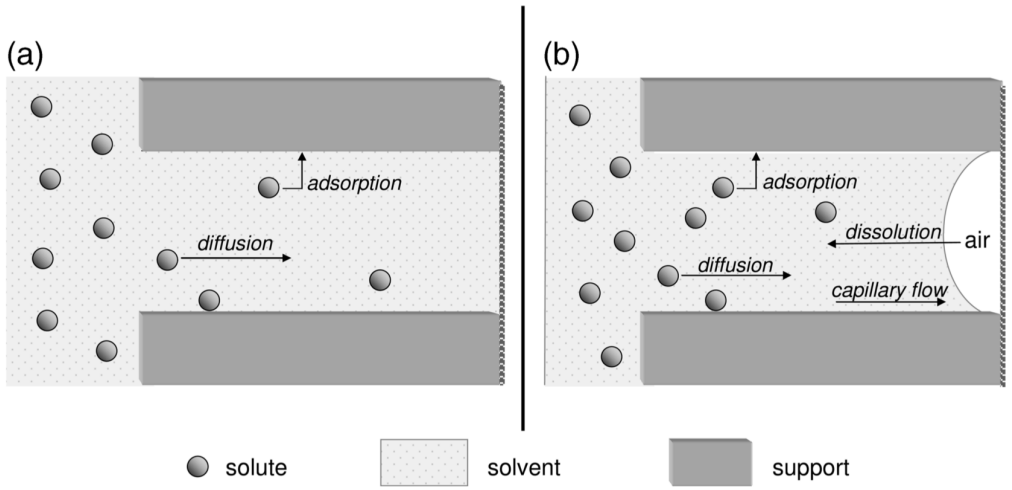

Figure 2.1: Illustration of wet impregnation (a) and dry impregnation (b) where the solute migrates into the pore from left to right [33].

The following step after impregnation is drying, which involves the elimination of the solvent from the pores, leading to an increase of precursor concentration up to saturation and crystallization. This step is also important if dispersion of the active material is favored. However, hydrated salt such as nitrate melts at moderate temperature, which can cause coalescence of the initially dispersed particles, or in worse case exclusion from pores. Normally the drying process is done by heating the sample up to the boiling point of the solvent, under a flow of gas or under static conditions.

2.3 Characterization methods

Theory behind the characterization techniques used in this project to determine catalyst properties is described in this section.

2.3.1 X-ray Diffraction (XRD)

X-ray Diffraction is one of the oldest and most frequently used technique for catalyst characterization. It is used to obtain an indication of particle size and identify crystalline phases inside the catalyst [34].

Solid matters are normally described as either amorphous, where atoms are arranged in random ways similar to the disorder found in a liquid. Glass is an example of an amorphous material. Or crystalline, where atoms are arranged in a highly ordered microscopic structure, forming a crystal lattice. About 95% of all solids can be described as crystalline [35].

The X-ray diffracted on a crystal plane allows one to derive the lattice spacing d by using Bragg relation:

$$n\lambda = 2d\sin\theta; \quad n = 1, 2, ... \tag{2.1}$$

Where n is an integer called the order of the reflection, λ is the wavelength of the incident X-ray beam and θ is the angle between the incoming X-rays and the reflecting lattice plane. Figure 2.2 illustrates the reflection of waves that hits a periodic lattice structure and forms interference patterns.

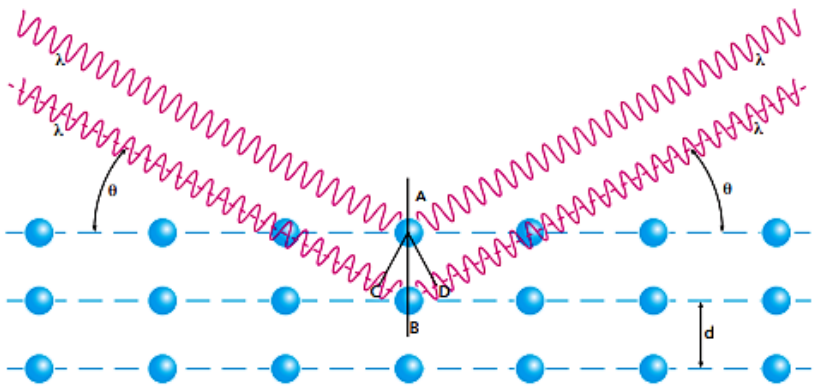

Figure 2.2: Demonstration of Bragg's law [36]

The first step in the evaluation of a XRD pattern is a qualitative analysis of the crystalline phases present in the sample. Different crystalline surfaces have characteristic diffraction peaks and by comparing the known reference compound to the Bragg diffraction peak one can determine the the crystalline phases. If the reference compound is not sufficient to explain the experimental pattern, there is a possible phase mixture present [37].

2.3.2 X-Ray Fluorescence (XRF)

X-ray fluorescence is an analytic technique used to determine the chemical composition of materials. The materials can be in powder, liquid, solid or other form. The method is non-destructive, fast and accurate, and requires only a minimum of sample preparation. XRF can be divided into two main groups: Wavelength Dispersive Systems (WDXRF) and Energy Dispersive Systems (EDXRF). The elements that can be analyzed and their detection levels depend on the system used. EDXRF has typical an elemental range from sodium to uranium, whereas WDXRF has a wider range, covering from beryllium to uranium. Elements with higher atomic numbers have better detection limits than lighter elements [36].

X-ray is generated when a sample is hit by an electron beam, and when the X-ray strikes an atom with sufficient energy, an electron is dislodged from the atom's inner shell. An electron from the atom's higher energy orbital shells drops to the inner shell and releases a photon. The energy is equal to the specific difference in energy between two quantum states of the electron. By measuring the intensities of the emitted energies it is possible to determine how much of each element is present in the sample. Figure 2.3 illustrates the electron dislodged by the X-ray photon, creating a characteristic fluorescent radiation.

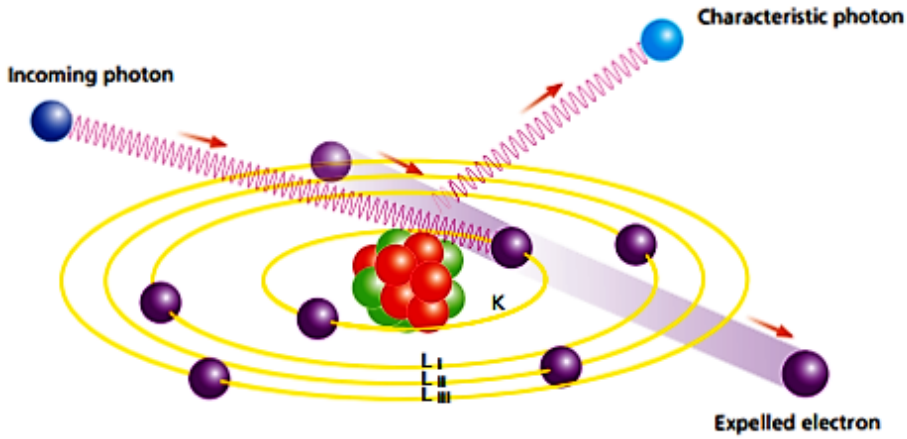

Figure 2.3: Illustration of a characteristic fluorescent radiation [36]

After a sample is measured, it is analyzed. First a qualitative analysis is done followed by a quantitative analysis. The qualitative analysis determines which elements are present and the measured spectra determines their net intensities. The net intensities are then used in the quantitative analysis to calculate the concentration of the elements. EDXRF uses the area of a peak to determine the intensity, while in WDXRF the height of the peak determines the intensity.

2.3.3 N_2 Physisorption

Physisorption is a term used to describe a weak interaction (van der Waal) between adsorbate and surface. Characterized by the lack of a chemical bond between the two, i.e. no electrons are shared. Gas molecules can physisorb on to a surface, and by knowing the specific area occupied by the molecule one can calculate the surface area of a sample. An adsorption isotherm curve can be obtained by plotting the amount of adsorbed gas volume against pressure, assuming that the surface is homogeneous, i.e no local difference in the adsorption enthalphy, the gas will first adsorb in a monolayer, completely covering the surface, before filling a new layer [38]. Nitrogen is an inert gas commonly used for this purpose, due to the well characterized adsorptive properties. By determining how many molecules are needed to fill the monolayer, and how much area the nitrogen molecule occupies, the total surface area can be calculated. Although simple, in practice, the molecules may adsorb beyond the monolayer to form multilayers, not limited to only the monolayer. The molecules can also condense in small pores, i.e. capillary pore condensation [39].

The type of isotherms produced may differ depending on the material. Figure 2.4 shows a schematic presentation of a type II isotherm, which is an idealized form of the adsorption isotherm for physisorption on a macroporous or nonporous solid. Where point ”B” is often taken to indicate the stage at which monolayer coverage is complete, and multilayer adsorption about to start [40].

Adsorption hysteresis appears in the multilayer range of physisorption isotherm. Figure 2.5 illustrates the characteristic features of a Type IV isotherm with its hysteresis loop. This is associated with capillary condensation in mesopore structures, and the limiting uptake over a range of high P/P_0. This type of isotherm is given by several mesoporous adsorbents, such as silica and alumina supports.

Hysteresis loops may exhibit different shape. Two extreme types are H1 and H4 shown in Figure 2.6. H1 has a vertical and nearly parallel branches over an appreciable range of gas uptake. Whereas H4 remain nearly horizontal and parallel over a wide range of P/P_0. Type H2 and H3 are considered the intermediate between these two extremes [40].

The shapes of the hysteresis loops are often identifiable with specific pore structures. Type H1 are often associated with porous materials known to consist of agglomerates or compact uniform spheres. Type H4, with similarities to H3 does not exhibit any limiting adsorption at high P/P_0. Typically observed with aggregates of plate-like particles giving rise to slit-shaped pores.

The Brunauer, Emmett and Teller (BET) is a widely used application to determine the surface area through its isotherms. BET isotherm is valid under certain assumptions [39]:

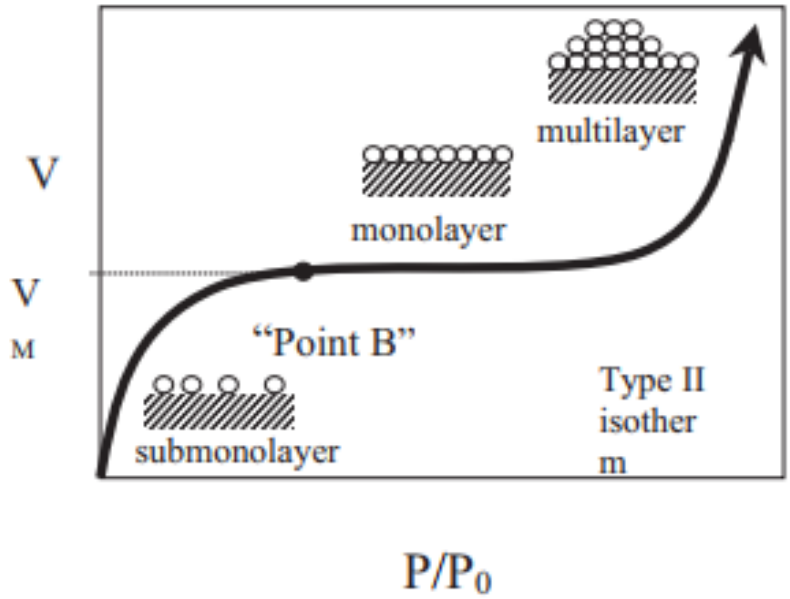

Figure 2.4: Schematic presentation of a Type II BET isotherm, observed with nonporous powders [40].

- The rate of adsorption and desorption in any layer are equal.
- Adsorbate-adsorbate interactions are ignored.
- Molecules adsorb on equivalent adsorption sites in the first layer.
- Molecules in the first layer constitute the adsorption sites for molecules in the second layers and higher.
- The adsorption-desorption conditions are the same for all layers but the first.
- The adsorption energy for molecules in the 2nd and higher layer equals the condensation energy
- The multilayer grows to infinite thickness at saturation pressure (P=P_0)

On the basis of these assumptions mentioned above, the BET isotherm (Equation 2.2) may be derived [39].

$$\frac{P}{V_a(P_0 - P)} = \frac{1}{\chi V_0} + \frac{\chi - 1}{\chi V_0}\frac{P}{P_0} \equiv \eta + \alpha\frac{P}{P_0} \tag{2.2}$$

here

$$\alpha = \frac{(\chi - 1)}{\chi V_0} \qquad \eta = \frac{1}{\chi V_0} \tag{2.3}$$

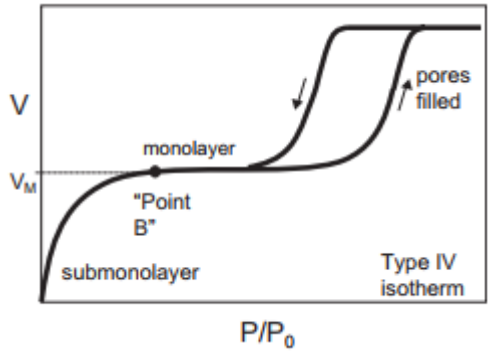

Figure 2.5: Schematic presentation of Type IV BET isotherm, typically observed for alumina and silica supports.

P_0 is the equilibrium pressure of the condensed gas, P the adsorption pressure, $\chi = k_2/k_1$ is the ratio of desorption rate constant for the first and second monolayer, V_a the total adsorbed gas volume and V_0 is the volume adsorbed in the first monolayer.

Plotting $\frac{P}{V_a(P_0-P)}$ against $\frac{P}{P_0}$ gives a linear plot with slope $\alpha = \frac{\chi-1}{\chi V_0}$ and a y-axis intercept $\eta = \frac{1}{\chi V_0}$. A simple rearrangement of these terms yields the volume of gas adsorbed in the first monolayer $V_0 = \frac{1}{\alpha+\eta}$. The ideal gas law can then be applied to approximate the amount of molecules, $N_0 = \frac{PV_0}{k_B T}$, adsorbed in the first monolayer. The total surface area can then be found: $A = N_0 A_0$, where A_0 is the area that each molecule occupies (typically N_2), and N_0 is the number of molecules adsorbed in V_0.

Due to the effects of capillary condensation, adsorbed gas may not necessarily desorb at the same pressure as adsorption. Therefore the effects of the capillary force has to be beaten in order for the adsorbed gas to desorb. This phenomenon is described by the Kelvin equation: (Equation 2.4)[41]

$$\ln\left(\frac{P}{P_0}\right) = -\frac{2\sigma\bar{V}\cos\theta}{rRT} \tag{2.4}$$

where σ is the surface tension of the adsorbate (liquid nitrogen), θ is the contact angle between liquid and surface, $\bar{V}$ is the molar volume of liquid nitrogen, r the pore radius, R is the universal gas constant and T is the temperature.

The Barret, Joyner and Halenda method uses nitrogen physisorption to calculate the pore size and the pore volume of a porous substance. By relating BET multilayer adsorption to capillary condensation phenomena [42]. The desorption pressure is dependant on the pore radius due to capillary condensation. The adsorbed multilayer has a specific thickness at a given pressure P/P_0, which can be determined empirically. The pore size distribution may be determined by relating the desorbed volume of gas at a pressure

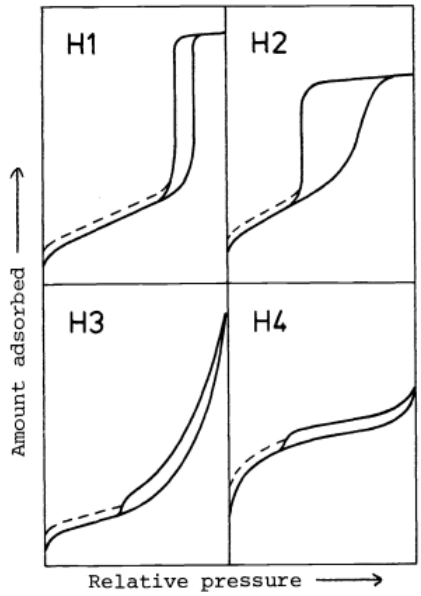

Figure 2.6: Types of hysteresis loops as defined by IUPAC [40]

P/P_0 to the adsorbant thickness and to capillary condensation. The method assumes that the adsorbate in the pores are only affected by forces of physical adsorption on the pore wall, capillary condensation in the pore volume and that the pores are cylindrical [42]

2.3.4 Thermogravimetric analysis (TGA)

In TGA, a sample is heated, or cooled according to a given temperature profile in a controlled atmosphere parallel to the weight changes of the sample being recorded.

Thermogravimetric analysis is the analysis of the mass of a sample versus temperature or time in a controlled atmosphere, usually coupled with a temperature program. It is a very useful technique implemented for any reactions related to a mass gain (oxidation, adsorption, wetting etc.) or a mass loss (drying, reduction, desorption etc.). TGA is normally coupled with other techniques to reveal mass conservative phenomena, such as phase transition. Differential scanning calorimetry (DSC) is one of the techniques normally coupled with TGA. When two or more techniques are applied to a single sample at the same time it is called a simultaneous thermal analysis (STA), such as TGA-DSC.

A TGA curve can then be obtained by plotting the weight change as a function of time and/or temperature, which can be used to establish information about thermally activated reactions expressed as weight change.

DSC uses heat to map physical or chemical processes that occurs over a range of temperatures [43]. It measures the change in the heat flow rate to a sample and to a reference sample, by both being subject to an identical temperature program, thus endothermic and exothermic reactions can be located. This STA makes it possible to obtain information regarding heat of transition, heat capacity and kinetic data on the sample.

2.3.5 Temperature Programmed Techniques

Temperature-programmed reaction methods are techniques in which a chemical reaction is monitored while the temperature increases linearly in time. Some of these methods include: temperature-programmed reduction (TPR), oxidation (TPO) and desorption (TPD).

The instruments involved in a temperature-programmed analysis is relatively simple. The reactor is charged with catalyst, which is controlled by a processor that heats the reactor at a linear rate of normally 0.1 to 20 °C min^{-1}. The composition of the outlet gas can be measured with a thermal conductivity detector or, preferably, a mass spectrometer.

In the TPR technique an oxidated catalyst undergoes a programmed temperature rise, while a reducing gas mixture is added (most commonly H_2 diluted in inert gas). TPR also provides information on the temperatures that is required for complete reduction of a catalyst.

The chemical reaction taking place during a temperature-programmed reaction (TPD/TPO) is represented by this general equation:

$$\mathrm{M_xO_{y\,(solid)}} + \mathrm{H_2} \longrightarrow \mathrm{M_{(solid)}} + \mathrm{H_2O} \tag{2.5}$$

The equation shows the reaction between a metal oxide and hydrogen, resulting in the production of the pure metal M and water.

2.3.6 Electron Microscopy

Electron microscopy is a straightforward technique used to determine the shape and size of supported particles [39]. Figure 2.7 illustrates what happens when a primary electron beam of energy around 100 to 400 keV hits a sample:

- Electrons can collide with atoms in the sample and be scattered back. This is called backscattering and becomes more effective as the atom mass increases. For instance, if a area of the sample contains heavier atoms than the surrounding area, it can be seen due to a higher yield of backscattering.

- Crystallographic information can be obtained when electrons are diffracted by particles favorably oriented towards the beam.
- Most transmitted electrons lose energy during interactions with the sample, this loss of energy can be analyzed by electron energy loss spectrometry. It provides information such as the elemental identity, chemical bonding, interacting atoms and surface properties.
- As a result, the interaction between the primary beam and the sample provides a lot of information on morphology, chemical composition and crystallography. Therefore making a projection of the sample density by using transmission electron microscopy is a routine way to study particle sizes in catalysts.

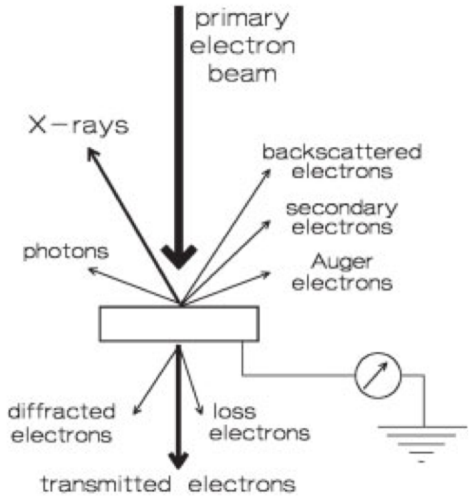

Figure 2.7: Illustration of the possible reactions when a primary electron beam of energy hits a sample [39]

Figure 2.8 shows how scanning and transmission electron microscopy (SEM and TEM) work. The TEM instrument is similar to an optical microscope, but with the optical lense replaced with an electromagnetic lense. A primary electron beam with high energy and high intensity passes through a condenser generating parallel rays that hits the sample. A bright field image is created from the magnification of a two-dimensional projection of the sample mass transmitted by the electrons. The dark field image is obtained from the diffracted electron beams. These beams are slightly off-angle from the transmitted beam.

Scanning electron microscopy (SEM) involves rastering a narrow electron beam over the surface of a sample and detecting the yield of either backscattered or secondary electrons as a function of the position of the primary beam. The contrast is caused by the orientation, where parts of the surface facing the detector is brighter than the parts pointing away from the detector. Secondary electrons have mostly low energies, around 5-50

eV, and originate from the surface of a sample. Backscattered electrons generally originate deeper and carry information about the composition of the sample, due to the more efficient scattering properties of heavy elements they appear brighter in the image.

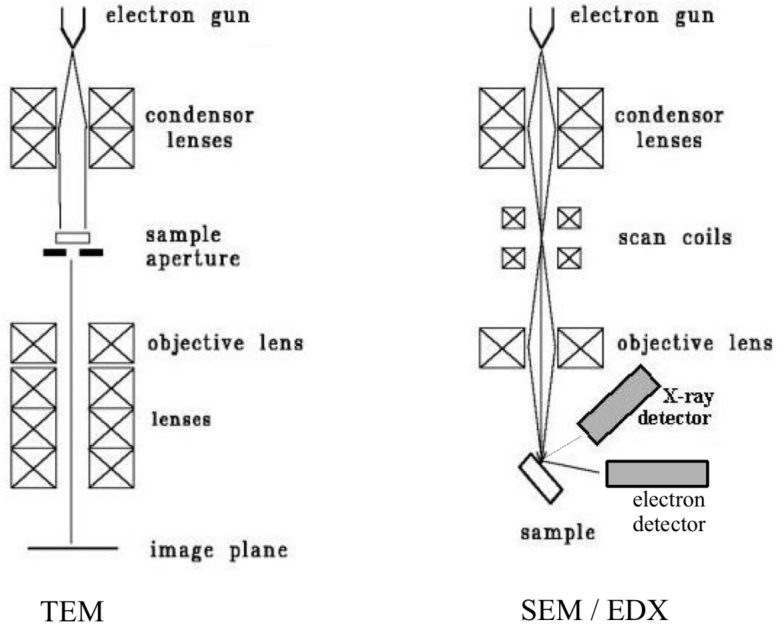

Figure 2.8: Illustration of how TEM works and how SEM/EDX works [39]

The resolution of a dedicated SEM instrument is about 5 nm, but can vary for instruments. The main difference between TEM and SEM is that SEM uses the topology and composition of a surface to determine contrast, while the electron beam in TEM projects all information on the mass it encounters as a two-dimensional image, but of subnanometer resolution [39].

2.3.7 Energy Dispersive X-Ray Spectroscopy

Energy-dispersive X-ray spectroscopy (EDS) is a powerful technique that is ideal for determining what elements and chemical compounds are present in a specimen. Similar to the XRF technique, EDS utilizes the photoelectric effect. The basic principle behind EDS consists of detecting the characteristic X-rays produced by each element. This is achieved by subjecting a sample with high energy electrons in an electron microscope. By utilizing a process known as X-ray mapping, information on elemental composition of a sample can then be overlaid on top of a magnified image of the specimen [44].

Another useful function of EDS is that the amount of X-rays emitted by each element

in a sample has a direct relationship with the concentration of that element (both atomic and mass fraction). This makes it possible to convert the X-ray measurements into a final X-ray spectrum and determine the concentrations of the various elements present.

Figure 2.9 illustrates a typical EDS system consisting of several key units. These include a main amplifier that provides amplification and a fast pulse inspection function to avoid pile-up events, and a semiconductor detector housed with a field-effect transistor (FET) preamplifier that is cooled to a sub-ambient temperature. This can be fully controlled with a computer assisted system, such as a computer-assisted X-ray analyzer (CXA), or a multichannel analyzer (MCA), allowing for automated and unattended operation [44].

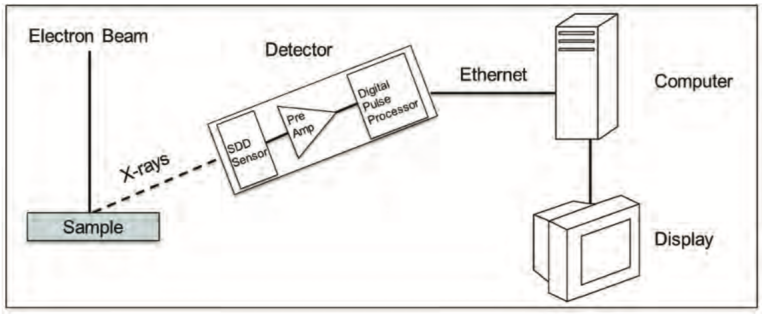

Figure 2.9: Illustration of a typical EDS system [44]

When a sample is hit by the electron beam, an X-ray will be generated. The X-ray escapes the sample and strikes the detector and creates a charge pulse. This current is then converted into a voltage pulse with a specific amplitude reflecting the energy of the X-ray detected. Lastly, the voltage pulse is converted into a digital signal and one more count is added to the corresponding energy spectrum. When the measurement is complete, the sum of all counts produce a typical X-ray spectrum with the major peaks shown on a background, as shown in Figure 2.10.

2.3.8 Mass Spectrometry

Mass spectrometry is an analysis method that ionizes chemical species and separates the ions according to their mass-to-charge ratio (m/z), and the intensity of each ions are then measured.

Three essential functions of a mass spectrometer are required to accomplish this. The ion source (1) in which the ionization of the molecules takes place. The most common and established method for ionization is electron impact. The molecules exited are bombarded by electron beam which removes an electron from the molecule, resulting in a charged ion. Electron impact normally produces single charged molecular ions and fragment ions, which are smaller parts of the original molecule. These ions are then accelerated into the

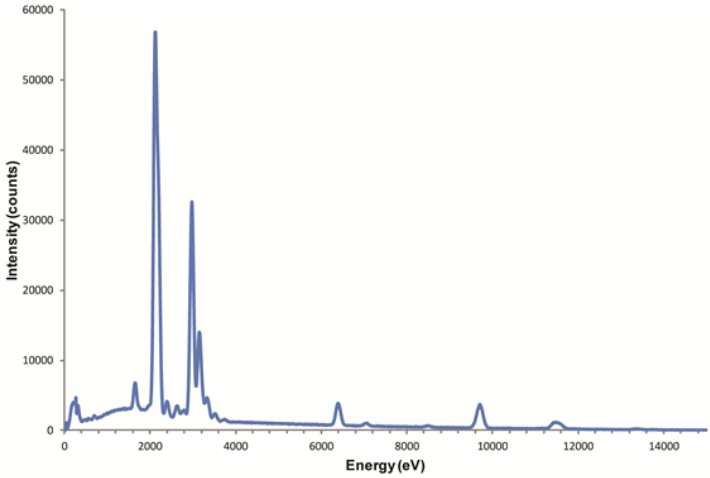

Figure 2.10: Illustration of a random EDS spectrum

mass analyzer (2) which sort and separates the ions according to their mass and charge values with the help of a magnetic field. At last, the detector (3) where the relative intensities (abundances) of the separated ions are determined and results displayed on a chart [45]. Figure 2.11 illustrates a typical mass spectrometer.

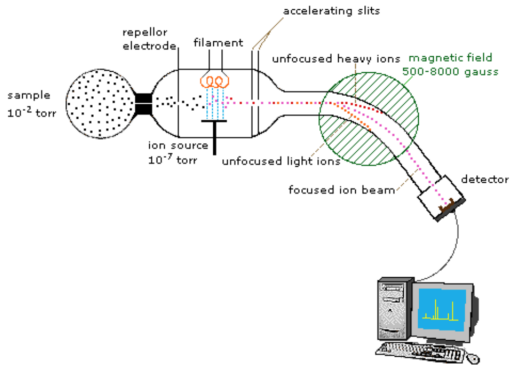

Figure 2.11: Illustration of the critical components in a typical mass spectrometer [45]

The instrument is operated at low pressure (high vacuum) by a system of oil diffusion or turbomolecular pumps. The low pressure permits the ions to travel from the ion source to the detector unimpeded with minimal interaction with other gas molecules. This prevents other gas molecules to scatter or fragment the ions and cause a reduction in sensitivity.

Calibration of the mass spectrometer is essential in retaining accurate measurements. A simple way to do this is a step-wise calibration. Where initially no gas (except for an inert) is fed to the MS and when a steady state is obtained, a known concentration of an

element or compound is fed to the MS and recorded over some time. The difference in signal (current) can then be calculated and correlated back to concentrations.

2.4 Activity test

Based on the background mentioned earlier, we know that the main reaction of NH_3-SCR is:

$$4\,NO + 4\,NH_3 + O_2 \longrightarrow {}_4N_2 + 6\,H_2O \tag{2.6}$$

The known elements and compounds present in the SCR reaction is summarized in Table 2.1. Where the mass spectrum is the mass to charge ratio detected by the mass spectrometer.

Table 2.1: Shows the elements and compounds found in a ammonia SCR reaction, with their respective mass to charge ratio.

Element/compound	Mass spectrum [m/z] (Fragment spectrum)
Hydrogen (H_2)	2
Ammonia (NH_3)	17 (16)
Water (H_2O)	18 (17)
Nitrogen (N_2)	28 (14)
Nitric oxide (NO)	30
Nitrogen dioxide (NO_2)	30 (46)
Oxygen (O_2)	32 (16)
Argon (Ar)	40

Combined with a calibration of the mass spectrometer the activity can be calculated for the catalyst tested.

The NO_x conversion is calculated as follows:

$$NO_x\text{-conversion} = \frac{[NO_x]_{in} - [NO_x]_{out}}{[NO_x]_{in}} * 100\% \tag{2.7}$$

Chapter 3

Experimental

This section covers the procedures, equipment, operating conditions and other parameters for experimental work performed for this project. Section 3.1 describes the experimental procedure for the preparation of the catalysts, while Section 3.2 covers the procedure of the various instruments used to characterize the catalysts. The amount of catalyst used in the characterization methods can be found in Appendix A.

3.1 Catalyst preparation

3.1.1 $CeO_2-ZrO_2-WO_3$

The first catalyst was prepared by hydrothermal synthesis, based on a procedure by Ning et al. (2014) [4]. All chemicals were of analytic grade. 1.16 g Zirconium(IV) oxynitrate hydrate (0.005 mol, Sigma-Aldrich), 2.17 g Cerium(III) nitrate hexahydrate (0.005 mol, Sigma-Aldrich) and 0.32 g Ammonium tungstate (Sigma-Aldrich) were dissolved in 1.5 mL acrylic acid (0.015 mol) and 0.05 molar glucose solution. Next, 12.5 mL of ammonia solution was added with vigorous stirring. The atomic ratio of Ce, Zr and W was 1:1:0.25 respectively.

The mixture was first aged for 5 hours at room temperature during continuous stirring, the resulting mixture was then transferred to a stainless autoclave and maintained a temperature of $160\,^{\circ}\mathrm{C}$ for 72 hours in an oven.

The autoclave was then cooled down to room temperature before the final solid product was filtered, washed three times with distilled water and dried at $80\,^{\circ}\mathrm{C}$ over night.

Finally calcined at $550\,^{\circ}\mathrm{C}$ for 5 hours in air with a temperature ramp rate of $1\,^{\circ}\mathrm{C\ min^{-1}}$. This catalyst was denoted as CZW and will be referred to as this throughout the report.

3.1.2 $CeO_2-ZrO_2-WO_3-Cu$

As several studies reported that catalyst like CeO_2 and ZrO_2, when loaded with small amounts of Cu enhances the SCR reduction of NH_3, it was desired to produce a similar catalyst with the addition of Cu. Therefore a second catalyst was prepared with the same procedure as CZW but with the addition of Copper nitrate. 0.698 g of Copper (II) nitrate hemi(pentahydrate), 0.323 g of Ammonium tungstate, 1.16 g Zirconium(IV) oxynitrate hexahydrate and 2.18 g of Cerium(III) nitrate hexahydrate were dissolved in 1.5 mL acrylic acid (0.015 mol) and 0.05 molar glucose solution. Followed by 12.5 mL of ammonia solution added during vigorous stirring. The desired ratio was still 1:1:0.25 with respect to Ce, Zr and W, and addition of 3 weight percent copper was desired.

The mixture was aged for 5 hours at room temperature and transferred to an autoclave and maintained a temperature of $160\,^{\circ}\mathrm{C}$ for 72 hours in a oven.

The solid product was then filtered, washed with distilled water and dried over right at $80\,^{\circ}\mathrm{C}$ over night, before calcined at $550\,^{\circ}\mathrm{C}$ for 5 hours in air with a temperature ramp rate of $1\,^{\circ}\mathrm{C\ min^{-1}}$. This catalyst was denoted as CZW-Cu.

3.1.3 $CeO_2-ZrO_2-WO_3$ with impregnated Cu

A third catalyst was produced through the same procedure as CZW. This catalyst was used as a support for the addition of 3% Cu through incipient wetness impregnation.

A sample of 0.4346 grams of the pre-calcined CZW sample was saturated with approximately 0.2 mL of a 50% methanol/water solution. This determined the volume required per gram of support to reach saturation to be approximately 0.46 mL/g.

0.0986 grams of copper nitrate was dissolved in 0.411 mL of the methanol/water solution. A pipette was used to apply the mixed copper nitrate solution drop-wise on 0.8942 grams of support. The mixture was then put in an oven and dried at $110\,^{\circ}\mathrm{C}$ with a ramp rate of $10\,^{\circ}\mathrm{C\ min^{-1}}$ for 10 hours.

The resulting solid was calcined at $550\,^{\circ}\mathrm{C}$ for 5 hours in air. This catalyst was denoted CZW-CuImpr.

3.2 Characterization

The catalysts were characterized by XRD, XRF, N_2 physisorption (BET), TGA, TPR, S(T)EM and EDS. Procedures, parameters and analysis conditions are presented in their respective subsections.

3.2.1 X-Ray Diffraction

XRD was used to determine crystallinity and the potential crystalline phase of the CZW, CZW-Cu and CZW-CuImpr catalyst. A powder sample was prepared and analyzed by a Bruker D8 Advance DaVinci instrument. With a Copper-anode, 0.1° divergence slit at 2θ between 20° and 80°, and wavelength λ = 1.54 Å for 2 hours.

Diffrac.Eva analysis suite was then used to process and analyze the obtained data.

3.2.2 X-Ray Fluorescence

XRF was performed for elemental analysis of the all three catalysts. Roughly 0.2 g catalyst and 3.0 g of a binder material (Boric acid, H_3BO_3) was mixed, grinded and pressed into a circular pellet for all the samples. A polypropylene film ($6\,\mu\mathrm{m}$) was used to cover the pressed pellet in the sample holder, which was then analyzed using a WDXRF Supermini 200 XRF apparatus for approximately 20 minutes.

3.2.3 N_2 Physisorption

A Micromeritics TriStar II instrument was used to perform BET physisorption. Approximately 0.2 g of catalyst sample was set under vacuum at $200\,^{\circ}\mathrm{C}$ overnight to desorb any adsorbed species in the sample. The sample was then installed in the instrument, where N_2 was used as the analysis gas. The sample was then evacuated and the analysis was performed in liquid nitrogen at temperature of $-195\,^{\circ}\mathrm{C}$.

3.2.4 Thermogravimetric analysis

Thermogravimetric analysis and differential scanning calorimetry was carried out on a Netzsch STA 449 C Jupiter instrument. 16 mg of the sample was placed in a sample holder and placed on a microbalance. The sample was heated in argon from room temperature with a rate of $5\,^{\circ}\mathrm{C\ min^{-1}}$ to $800\,^{\circ}\mathrm{C}$, while TGA and DSC data were measured simultaneously along the increasing temperature. The software Netzsch-TA45 (Proteus) was used for the analysis of the DSC and TGA results. This procedure was performed for all three catalysts.

3.2.5 Temperature Programmed Reduction

A TPX Altamira BenchCAT Hybrid was used to perform TPR, with 7% H_2 in argon and a temperature ramp rate of $10\,^{\circ}\mathrm{C\ min^{-1}}$ to $900\,^{\circ}\mathrm{C}$. Approximately 100 mg of sample was weighed and prepared in a quartz u tube reactor before inserted into the apparatus. The same program was ran for all three catalysts.

3.2.6 S(T)EM and EDX

A Hitachi S-5500 S(T)EM was used to obtain details about the structure of the catalysts. Different acceleration voltages ranging from 15-30 kV and beam currents ranging from 5-20 µA were utilized to obtain images with high resolutions.

A Bruker EDX system is utilized along with the S(T)EM to allow for the elemental mapping of the different catalysts. The images are taken by selecting an area of interest from the sample and mapping the elemental species.

3.3 Activity test

Before performing activity test on the catalysts a calibration of the MS was performed. The purpose of this calibration was to ensure correct measurements during the activity

tests, while also being able to correlate the signals with concentrations. This way the conversion of the catalyst tested could be determined. MS is not a typical equipment used for the activity tests, and therefore the correlation from ion current to concentration might not be as accurate. Since the MS signals might vary from day-to-day, a perfectly accurate MS calibration might still differ slightly for the day the catalysts were tested. Therefore it is assumed that the calibration is valid for all the tests. The calibration plot is shown in Figure 3.1, where only few selected masses are represented. These are; NO, O_2, Ar and NH_3. These were the input gases used in the activity tests and therefore the most relevant to observe since they were control variables. An empty quartz capillary reactor was installed during the calibration.

The procedure for the calibration:

- 0-60 min: Start-up with no gases fed to the system, waiting for the signals to stabilize.
- 60-120 min: Argon was introduced to the system and kept constant for an hour.
- 120-190 min: Argon was closed off and 10% O_2 was added to the system.
- 190-250 min: The O_2 stream was closed and 600 ppm NO was added to the system.
- 250-330 min: NO was shut off while 600 ppm of NH_3 was introduced to the system.

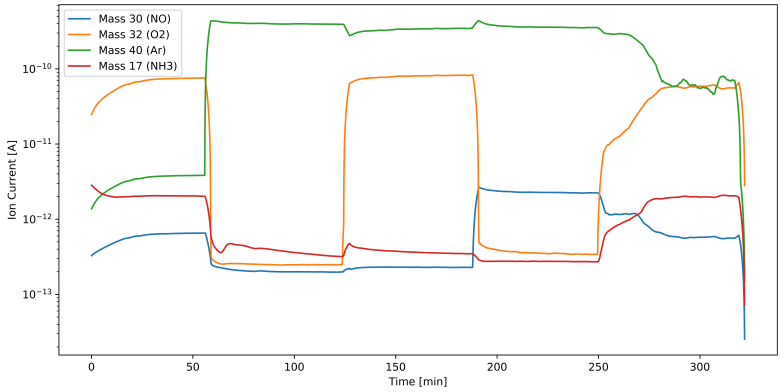

Figure 3.1: MS calibration graph with the 4 different gases, NO, O_2, Ar and NH_3 tested during calibration of MS.

From the calibration graph, the initial 60 minutes where no gas was fed reaches a steady-state signal. The average of the last 30 minutes of steady signal is then used as point zero for argon. After argon is fed (shown as the green line) the last 30 minutes during the

steady-state signal is then taken and averaged. The difference in the signal can then be used to correlate the signal with the known concentration of argon added.

The challenge with using a mass spectrometer to determine the concentration of the reactants/products are due to the overlapping mass spectrum. For instance, NH_3 has both mass 16 and 17 with relative high intensity, which is overlapping with H_2O that has a mass spectrum of mass 17 and 18 [46]. Thus making it hard to determine the exact contribution of ion current related to each element. The only element that has a distinctive mass is NO with mass 30. Therefore making it the easiest and most relevant element to base the calibration on. NO_2 was disregarded due to the low ion current signal observed during the SCR reactions.

Figure 3.2 shows the calibration plot for NO concentration, which will be used to determine the activity of the catalysts. The zero-value point is taken from the average 20 minutes from 150-170 minutes in Figure 3.1, and the first value point is the average 20 minutes between 230-250 minutes. The two points are assumed to have a linear correlation and will be used to determine the concentration of NO after the SCR reaction for all the catalysts. The linear equation obtained from the calibration was found to be:

$$y = 3 * 10^{-15}x + 2 * 10^{-13} \tag{3.1}$$

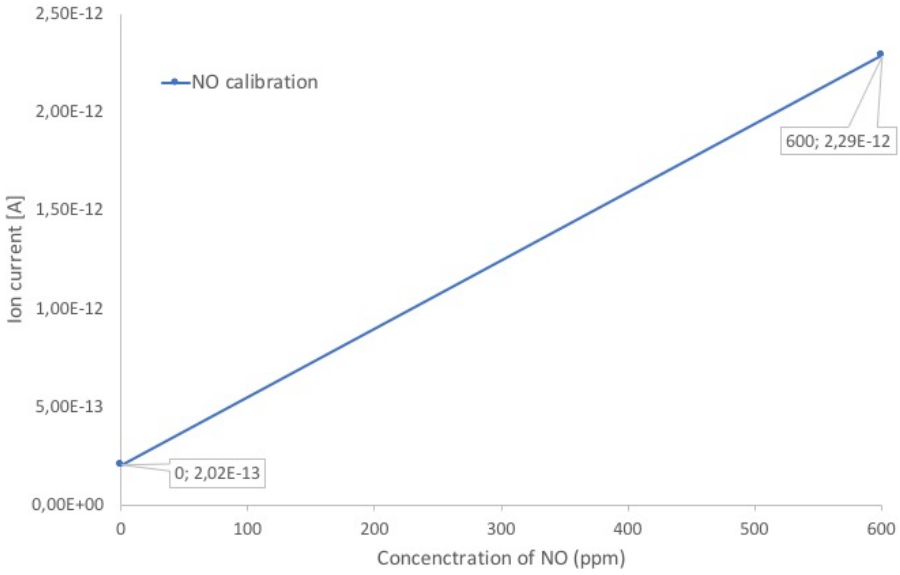

Figure 3.2: Calibration plot for NO. Assuming a linear correlation based on a zero-value point (0 ppm signal) and first-value point (600 ppm signal).

Catalytic activity for SCR of NO was carried out in a capillary reactor made of quartz glass (1.5 mm outer diameter, 0.01 mm wall thickness). Figure 3.3 shows the set-up of the reaction system, where a Pfeiffer Vacuum MS-instrument was ran with Quadera to measure the change in ion current for the various components. The mass flow controllers (MFC) were connected to a computer to ensure good flow control and the MS was connected to a separate computer to record the change in signals over time.

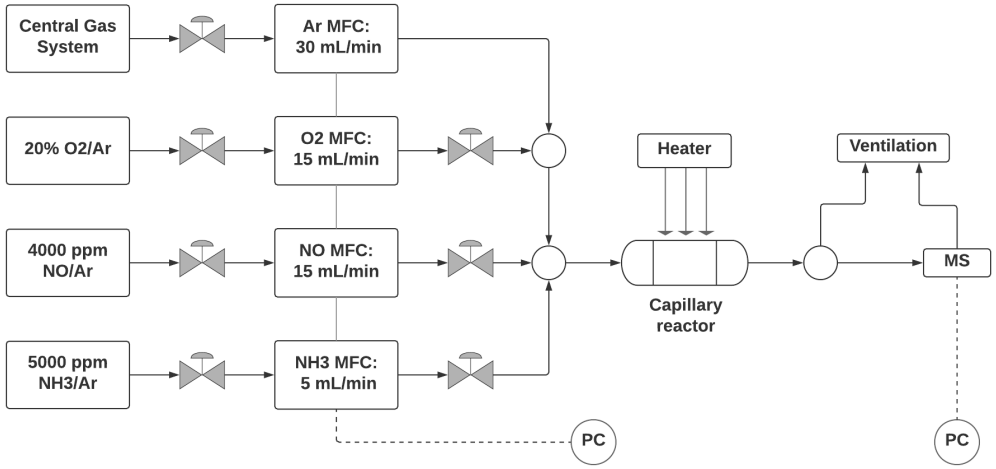

Figure 3.3: Process flow diagram of the reaction system.

The catalysts were prepared into the capillary quartz glass reactor with glass wool on both sides of the tube, keeping the catalyst in place. The glass reactor was then thread through a holder, sealed with glue and mounted on the set-up. A picture of the glass reactor mounted on the holder is seen in Figure 3.4.

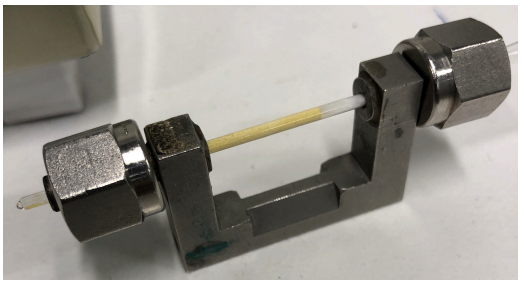

Figure 3.4: Picture of the quartz glass reactor threaded in a holder

Calibration of the mass spectrometer was performer in order to determine the concentrations of products and reactants after the SCR reaction. An empty capillary reactor was placed on the set-up and zero gas was fed to the system initially.

3.3.1 CZW Procedure

The procedure for the CZW catalyst activity was performed by flushing the reactor with argon while raising the temperature to 350 °C. After the temperature reached 350 °C, it was lowered to 250 °C while 600 ppm NO and 10% O_2 were added to the system. This was maintained for roughly an hour, followed by the addition of 600 ppm NH_3.

After another hour and the signals had stabilized, the NH_3 was turned off, and temperature was lowered to 200 °C. When the signals stabilized and the temperature was reached, 600 ppm ammonia was introduced again. The same procedure was done for 150 °C. Argon was adjusted throughout the run to maintain a total flow of 30 mL.

3.3.2 CZW-Cu Procedure

The catalytic activity for NO reduction was carried out by flushing the catalyst with argon at room temperature to ensure that only inert gas was present before any other gas was fed to the system. The temperature was then raised to 350 °C with a ramp rate of 10 °C min^{-1} to activate the catalyst.

After the activation the temperature was reduced to 250 °C followed by an addition of 10% O_2 and 600 ppm NO. After a while, 600 ppm of NH_3 was added to monitor the SCR reaction. Argon was adjusted throughout the run to maintain a total flow of 30 mL.

The same procedure was done at 200 °C and 150 °C.

3.3.3 CZW-CuImpr Procedure

The same procedure was carried out on the CZW-CuImpr catalyst as the CZW catalyst. Where argon was used as an inert gas to maintain a total flow of 30 mL and used to flush the sample at the beginning.

The temperature was raised to 350 °C to activate the catalyst with only argon. Reduced the temperature to 250 °C and introduced 600 ppm NO and 10% O_2, maintained for an hour before 600 ppm NH_3 was introduced. After another hour and the signals had stabilized, the NH_3 was turned off, and temperature was lowered to 200 °C. When the signals stabilized and the temperature was reached, 600 ppm ammonia was introduced again. The same procedure was done for 150 °C.

Chapter 4

Results and discussion

Results from the characterization and other analysis of the CZW, CZW-Cu and CZW-CuImpr samples are presented in this section. The results and discussions are separated into their respective sections based on the method.

4.1 X-Ray Diffraction

XRD was used to determine the crystallinity and structure of the samples. The diffractogram from the XRD analysis is shown in Figure 4.1. XRD also served the purpose of determining which chemical bonds were formed in the samples by looking at diffraction patterns.

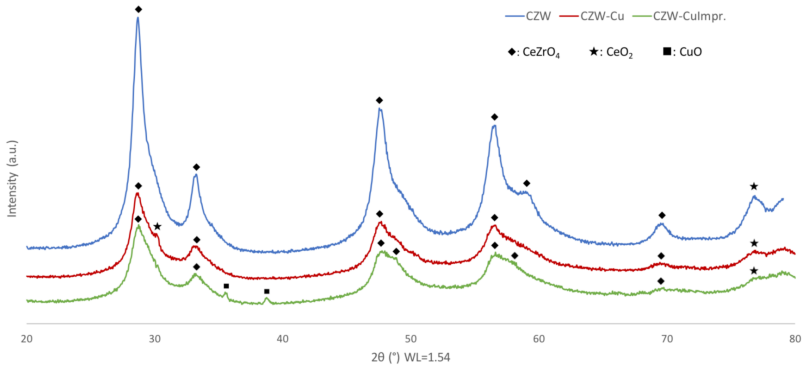

Figure 4.1: XRD diffractogram of the catalysts. The diamond shape indicates the $CeZrO_2$ peaks, while the star shape indicate CeO_2 peak and the square indicates the CuO peaks. Each sample has an arbitrary unit, but were analyzed with the same parameters and therefore directly comparable.

All the samples show typical diffraction peaks for the cubic fluorite structure of $CeZrO_4$ and CeO_2 (Appendix B).The position of the peaks are slightly shifted to the left compared to the reference file. No obvious peaks attributed to the crystalline phase of WO_3 was observed in any of the CZW-based catalysts. Indicating that WO_3 exists as a highly dispersed species. The diffraction peaks of $CeZrO_4$ also gradually decrease for all samples.

The diffraction peaks are rather broad. For CZW, this indicates that the Ce, Zr and W species show characteristics of poor crystallization and well distributed. A correlation between the WO_3 content and the intensity of CeO_2 peaks was reported by Song et al. [9], where a concentration of more than 20% WO_3 decreased the intensity of CeO_2 peaks and favoured the formation of CeO_2-ZrO_2 solid solution. Where the amorphous WO_3 would cover the catalyst surface and consequently decrease the intensity of CeO_2 peaks.

The same property is further enhanced for the Cu containing samples, where the intensity of the peaks are further decreased. As the concentration of Cu was roughly 3%, it further dispersed on the surface of the catalyst, resulting in decreased intensity of CeO_2. A characteristic peak for CuO was found in the CZW-CuImpr sample, indicating a different surface characteristic compared to the CZW-Cu sample.

4.2 X-Ray Fluorescence

XRF was used to determine the elemental composition of the samples. The results are presented in Table 4.1. A sample of the support used in the CZW-CuImpr catalyst was also tested to compare the composition before and after the addition of Cu.

Table 4.1: Results of XRF analysis of CZW, CZW-Cu and CZW-CuImpr. The elemental compositions are presented as the presumed oxide, as the XRF instrument is not able to determine oxides. The mass percentage also does not add up to 100, since minor compounds are ignored.

Sample	Compound	Mass Percentage [%]
CZW	CeO_2	51.9
	ZrO_2	31.1
	WO_3	14.6
CZW-Cu	CeO_2	46.7
	ZrO_2	32.3
	WO_3	16.6
	CuO	4.4
CZW-CuImpr	CeO_2	41.0
	ZrO_2	35.6
	WO_3	19.1
	CuO	4.2
CuImpr-Support	CeO_2	41.4
	ZrO_2	39.2
	WO_3	19.4

Since XRF assumes the composition of the sample to only contain its respective metal oxides, a recalculation was necessary. The purpose of the calculation was to check the desired molar ratio of Ce, Zr and W being 1:1:0.25 respectively. For the Cu samples, a 3 mass percentage Cu was the desired amount. Table 4.2 shows the resulting amount of the elemental metals, where values from Table 4.1 are used in the calculation.

Table 4.2: The amount of the elemental metals in the sample based on 1 gram sample. The calculations were done by choosing 1 gram as the basis for the calculation. Resulting in 0.519 gram CeO_2 for CZW, which was then divided by the molar mass of the metal. The same method was used to calculate the other compounds.

Sample	Comp.	Mol. mass of metal	Mol calc.	Ratio (Relative to Zr)
CZW	CeO_2	140.0 [g/mol]	0.0037	0.91
	ZrO_2	91.2 [g/mol]	0.0034	1
	WO_3	183.8 [g/mol]	0.00079	0.23
CZW-Cu	CeO_2	140.0 [g/mol]	0.0033	0.94
	ZrO_2	91.2 [g/mol]	0.0035	1
	WO_3	183.8 [g/mol]	0.00090	0.26
	CuO	63.55 [g/mol]	0.00069	0.19
CZW-CuImpr	CeO_2	140.0 [g/mol]	0.0029	0.74
	ZrO_2	91.2 [g/mol]	0.0039	1
	WO_3	183.8 [g/mol]	0.0010	0.26
	CuO	63.55 [g/mol]	0.00066	0.17
CuImpr-Support	CeO_2	140.0 [g/mol]	0.003	0.70
	ZrO_2	91.2 [g/mol]	0.0043	1
	WO_3	183.8 [g/mol]	0.0011	0.26

The molar concentration of Zr was used as basis to calculate the ratio. All the ratios are very close to the aim of 1:1:0.25 ratio, with the only exception found in the CWZ-CuImpr sample, where the concentration of Ce seems a bit lower than what is desired. The XRD of CZW-CuImpr also showed that less CeO_2 signal was observed. This result might indicate that the support synthesized in the CZW-CuImpr is different than the CZW sample. This was confirmed by the XRF analysis of the CuImpr-Support, which had a ratio of 0.7:1:0.26 for Ce, Zr and W respectively. This resulted in a undesired atomic ratio between the metal species and have direct consequence on the morphology of the CZW-CuImpr catalyst. As the most dominant structure is based on the chemical structure of $CeZrO_4$, the unbalanced concentration of Ce and Zr might limit the formation of the desired structure.

For the Cu samples, the desired mass percentage was 3 for both samples. Definition of mass percentage:

$$\frac{\text{Mass of metal}}{\text{Mass of compound}} * \text{Mass percentage} \tag{4.1}$$

For CZW-Cu: $\frac{63.55}{79.55} * 4.4 = 3.52$, and CZW-CuImpr: $\frac{63.55}{79.55} * 4.2 = 3.36$. Both samples were marginally above the desired percentage, but not significant.

Based on these XRF results, the goal of synthesizing catalyst with the desired ratio between Ce, Zr and W was achieved for the CZW and CZW-Cu sample. The slightly lower Ce content on the CZW-CuImpr catalyst might have affected the morphology of the catalyst and changed the performance of the catalyst.

4.3 N_2 physisorption

The BET surface area, BJH pore size and pore volume obtained from N_2 adsorption/ desorption analyses are shown in Table 4.3. All the results presented in the table regarding surface area, pore size and pore volume are based on data from Appendix C. Calculations are based on the assumptions given earlier in subsection 2.3.3.

Table 4.3: Results from N_2-physisorption, where BJH desorption volume and pore size are used.

Sample	BET surface area $[m^2/g]$	Pore volume $[cm^3/g]$	Pore size [nm]
CZW	62	0.098	6.4
CZW-Cu	76	0.075	3.6
CZW-CuImpr	42	0.081	6.2

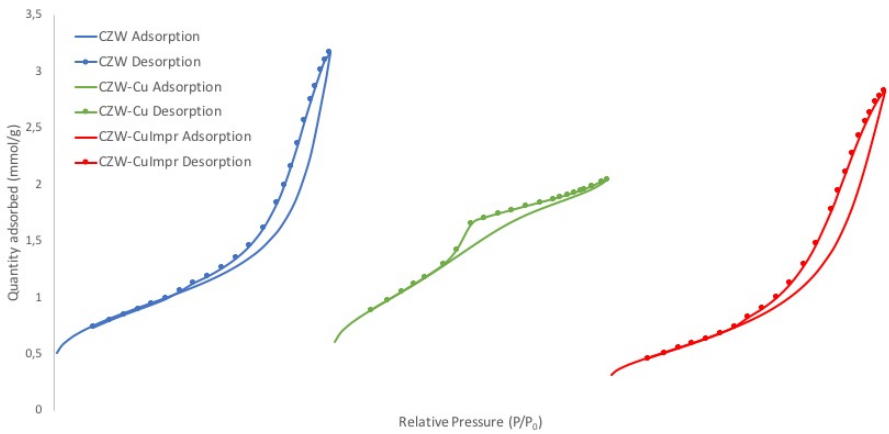

Figure 4.2: Comparison of the three isotherms and their quantity adsorbed. The relative pressure on the x-axis goes from 0 to 1 for all the catalysts.

The BET isotherm is shown in Figure 4.2 and Figure 4.3, while the BJH desorption plot is presented in Figure 4.4.

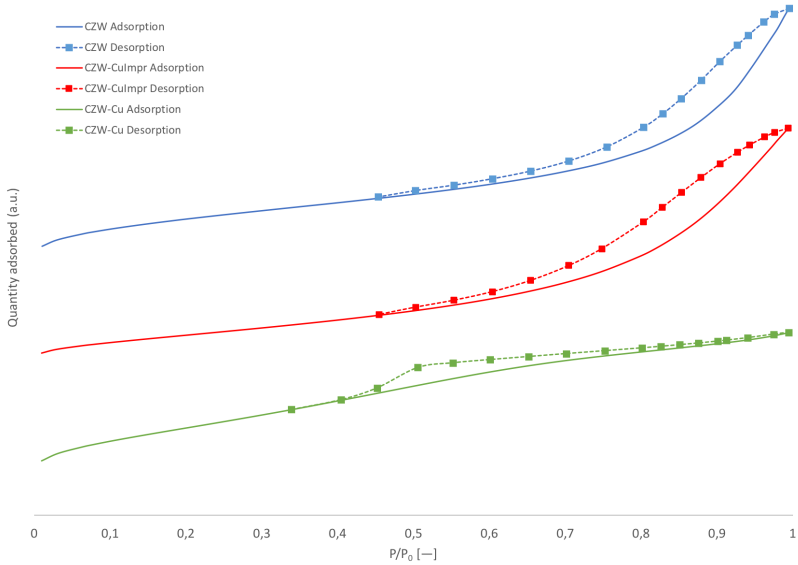

Figure 4.3: BET plot of the three catalyst, showing the obtained isotherms for adsorption and desorption.

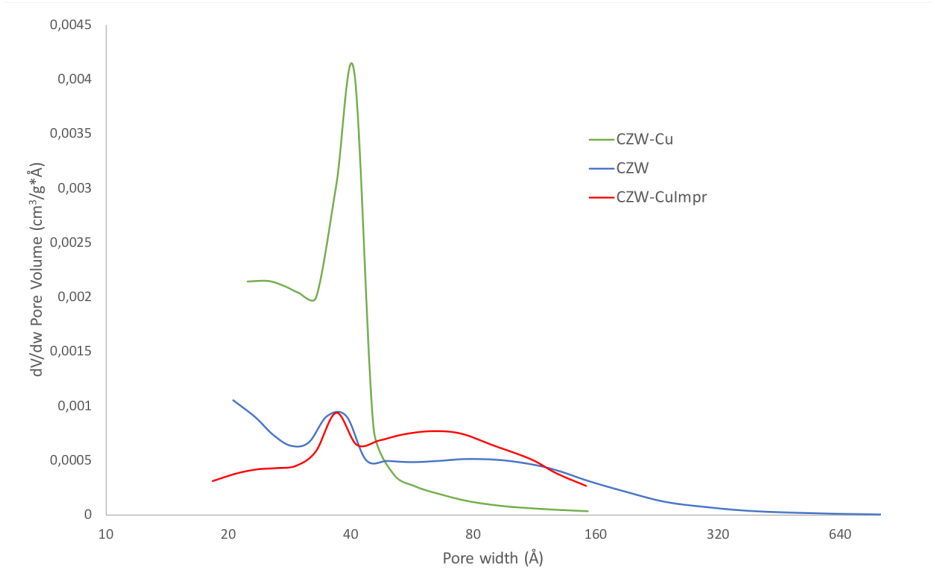

Figure 4.4: BJH desorption analysis for the three catalysts. The x-values are plotted on a logarithmic scale, showing the distribution of pore volume for a range of pore size.

From the BET plot we can see that the isotherm and hysteresis is quite similar for the CZW and CZW-CuImpr catalysts. They are both quite narrow, but covers a large range of P/P_o, indicating that there is a wide range of pore size and that adsorption and desorption occurs over a large pressure range. The isotherm indicates a type II isotherm previously illustrated in Figure 2.4, showing no adsorption limitation at high relative pressure. This also indicates that the adsorbent do not possess well-defined mesoporous structure.

For the CZW-Cu sample a very different isotherm emerges. At lower pressures the adsorption isotherm behaves similar to the two other catalysts, where the monolayer is filled first followed by multilayer adsorption. But as the monolayer is filled and the multilayer is starting to fill, the CZW-Cu catalyst seem to be unable to fill multilayer, resulting in a hysteresis similar to H4 as shown in Figure 2.6. The isotherm indicates a type I isotherm, indicative of mesoporosity and microporosity as defined by IUPAC [40].

From the BJH plot, we can see that the similarity from the isotherms of CZW and CZW-CuImpr is further reflected on the pore size distribution and pore volume. The CZW catalyst seem to have a wide range of pore sizes, ranging from around 2 nm to 32 nm. The CZW-CuImpr catalyst also possess a wide range of pore sizes, ranging from 2 nm to 16 nm. These resulting in average pore size of 6.4 nm and 6.2 nm for CZW and CZW-CuImpr respectively. The lower surface area of CZW and CZW-CuImpr also indicate less porosity in the catalysts.

For the CZW-Cu sample, a well defined BJH curve where the pore size ranged from around 2 nm to 8 nm was observed. Where the majority of the pore volume and size were distributed around the 4 nm pores. This average pore size obtained was 3.6 nm, while the BET surface area was found to be 76 m^2 g^{-1}. For comparison, the CZW and CZW-CuImpr samples had a surface area of 62 and 42 m^2 g^{-1} respectively. Indicating that the CZW-Cu sample is more porous than the two, giving rise to a larger surface area.

4.4 Thermogravimetric Analysis

Results from the TGA analysis of all the three catalysts are shown underneath. Figure 4.5 shows the mass loss of the samples over a temperature profile up to $800\,^{\circ}\mathrm{C}$ with a ramp rate of $10\,^{\circ}\mathrm{C}$ min^{-1}.

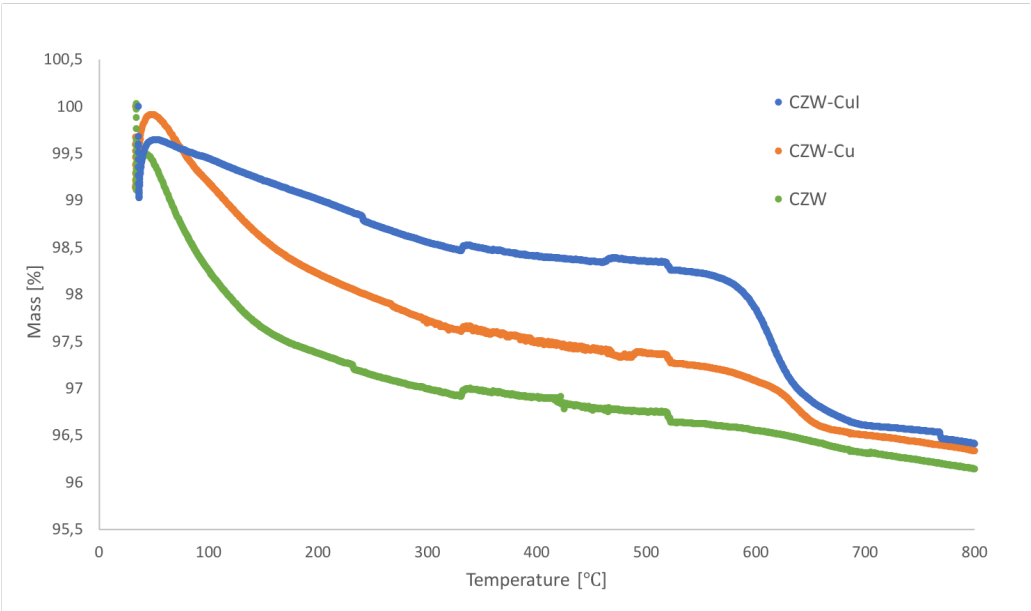

Figure 4.5: Mass loss versus temperature for CZW, CZW-Cu and CZW-CuImpr

From the graph, we can see that all three catalysts have a similar mass loss curve, with CZW sample having the highest mass loss of approximately 3.9 %, and CZW-CuImpr the lowest with roughly 3.5 %. This loss of mass in all the samples early can be contributed to vaporization of water. Apart from that, all the catalysts shows stable thermogravimetric curve. The catalysts are stable up to a temperature around 550 °C, where this was the calcination temperature of the catalysts. The mass loss above the calcination temperature will be irrelevant for the catalyst activity, and therefore not discussed further.

Figure 4.6 shows the DSC changes over the same temperature profile for all samples. From the DSC curve we can see that the amount of heat required to heat the temperature of the sample is stable for all the samples to 500 °C. After this temperature the CZW sample indicates an exothermic phase transition reaction, where less heat is required to increase the temperature to around 650 °C. For the two copper containing samples, they have a similar curve, with CZW-CuImpr, having a slightly lower heat requirement. The exothermic phase transition registered on the CZW and later for CZW-CuImpr can be speculated to have something to do with the phase transition of the mixed oxides [47]. Despite this, the temperature where the catalyst will be operating (150-250 °C), indicates thermally stable catalysts.

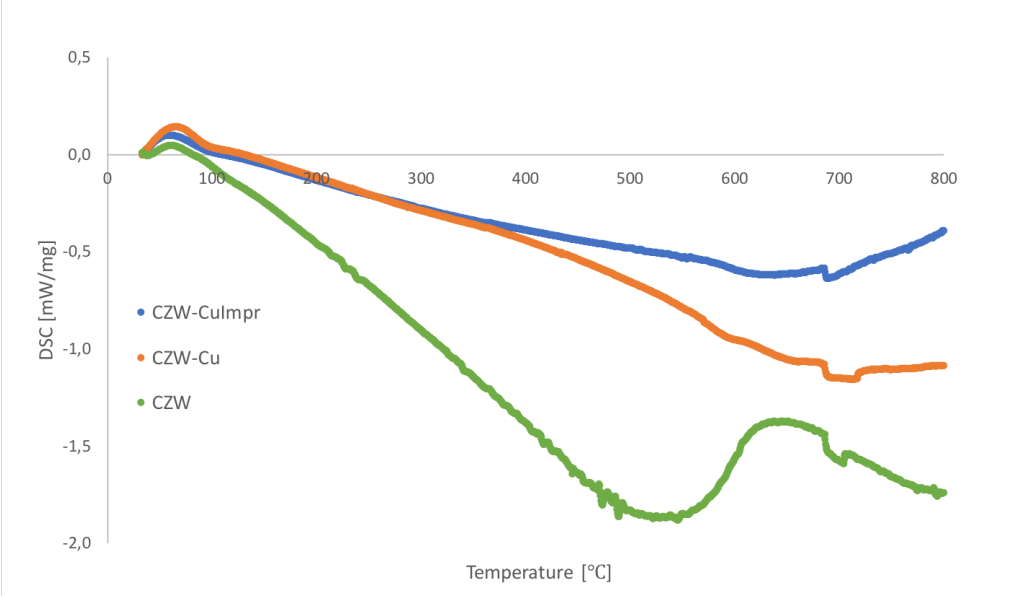

Figure 4.6: DSC signals versus temperature for CZW, CZW-Cu and CZW-CuImpr. Showsing the thermal stability of the samples, where CZW requires more energy to raise its temperature compared to CZW-CuImpr.

4.5 Temperature Programmed Reduction

Temperature programmed reduction was performed on the catalysts and the results are presented in Figure 4.7.

No observable reduction peak is observed for the CZW sample, indicating no redox reactions for the catalyst.

For the Cu containing catalysts on the other hand, a peak was observed for both of the catalysts around the temperature of 200-300 °C. These are also temperatures reported to be normal for the reduction of Cu [48, 49]. The most distinct peak is the one from the CZW-Cu sample, where the temperature range of the reduction and oxidation occurs between roughly 200-250 °C. Indicating a faster reduction and oxidation reaction for the catalyst at a narrow temperature range. The reduction peak at 200 °C is reported to be the reduction of isolated Cu^{2+} to Cu^{1+}, and reduction of CuO clusters [49]. The broader and lower peak for the CZW-CuImpr sample indicates a slower reaction and less reducible Cu, where the reduction peak around 280 °C is reported to be the reduction of Cu^{1+} to metallic Cu [50].

For CZW-Cu sample, this could have a positive effect on the activity, as Cu is said to enhance the SCR of NH_3, and by showing that the sample has an active redox reaction at

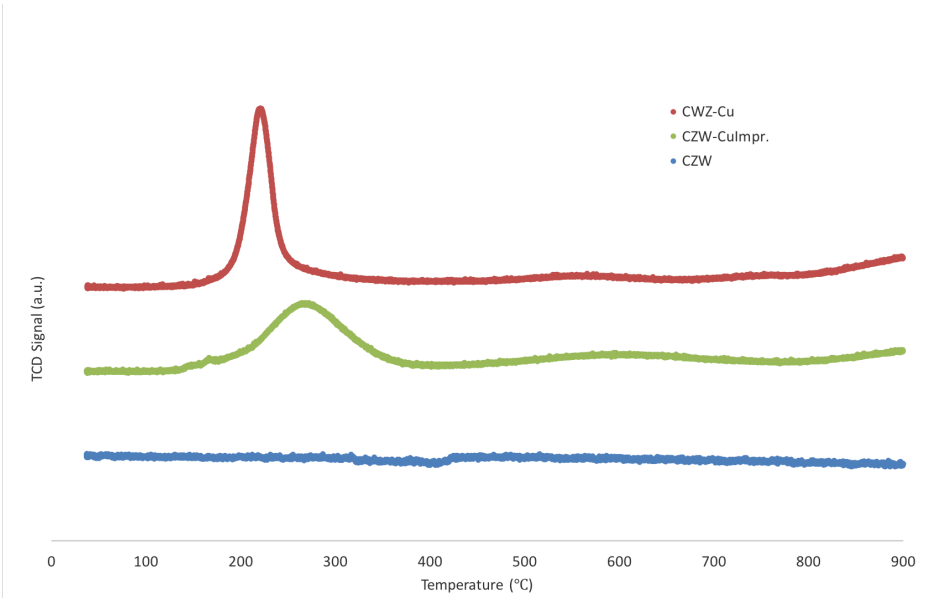

Figure 4.7: TPR analysis of the catalysts ran on the same parameters and temperature profile.

the relevant temperature makes this promising.

The same thing can be said for the CZW-CuImpr catalyst, but the effect on the SCR activity has to be tested in order to confirm the more effective catalyst. It can be speculated that the CZW-CuImpr sample will have lower impact on the Cu effect, due to the smaller and broader peak which is also at a higher temperature range.

4.6 S(T)EM and EDS

S(T)EM was used to obtain more detail about the structure of the catalysts. While EDS gave further insight on the surface species and distribution, which can further confirm results given from the other characterization techniques used.

4.6.1 CZW

A sample of the CZW catalyst was used to obtain SEM images shown in Figure 4.8. Figure 4.8(a), shows catalyst particle with uneven size and morphology. It also shows broken spherical particles, which also were observed elsewhere on the sample.

Figure 4.8(b) is the surface of one of the spheres observed, where we can see numerous ”rifts” formed on the surface with different shapes and diameters. It was speculated that

these rifts were related to the results given from BET, where the pore diameters ranged from 2 nm to 32 nm. Because the BET data indicated a wide range of pore diameters similar to rifts observed, it could be one of the explanations behind the BET data obtained, but this could not be confirmed due to limitations on the SEM.

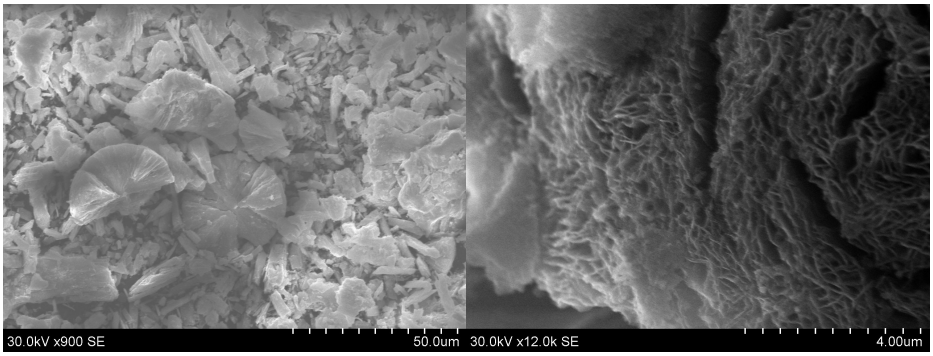

(a) **(b)**

Figure 4.8: SEM images of CZW sample, where (a) is a selected area on the sample, and (b) is a close-up image of a selected spherical particle not shown in (a). Similar surfaces was observed throughout the sample.

EDS was used on the same sample to give insight on elemental composition on the surface. The images obtained by the EDS is shown in Figure 4.9, where an area of interest (surface of a spherical particle) was used to analyze the distribution of elements. The image to the left (a) is the selected area of interest, which is just the surface of one of the spherical particles containing the rifts, while the image to the right (b) is the elemental mapping done by the EDS. It can be seen that the distribution is rather homogeneous which is a desired characteristic for the catalyst.

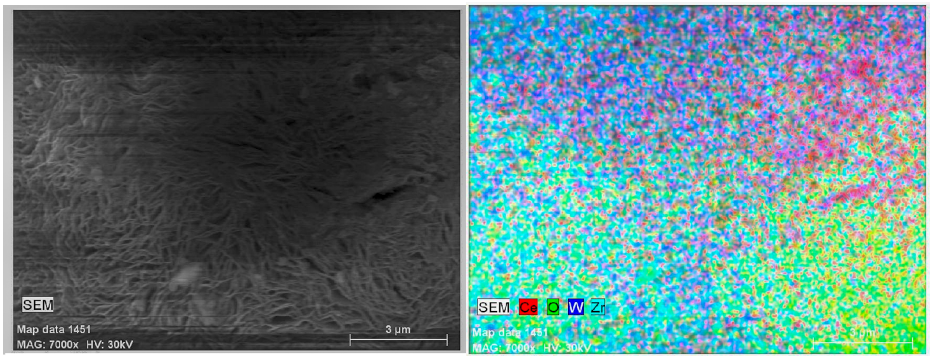

(a) **(b)**

Figure 4.9: EDS image of CZW, where (a) is the surface of a randomly selected spherical particle. (b) is the elemental mapping of the selected image (a).

4.6.2 CZW-Cu

SEM images from the CZW-Cu sample is shown in Figure 4.10. On the image to the left (a), spherical particles with similar sizes were found throughout the sample. Smaller and different shapes of particles were also seen, and seems to be particles originating from the spherical particles. These spherical particles contributes to a larger specific surface area from the BET due to their larger sizes as shown in Figure 4.10(a). Since BET takes the average surface area based on all the particles, these spherical particles will contribute more than the smaller particles.

Image (b) to the right is a close-up picture of one spherical particle (circled red in (a)). Similar to the CZW sample this one also has numerous rifts on the surface, but in a denser formation. Given the same catalyst synthesis method this might explain the similarity. The diameter of the spheres were estimated to be around $35\,\mu\mathrm{m}$.

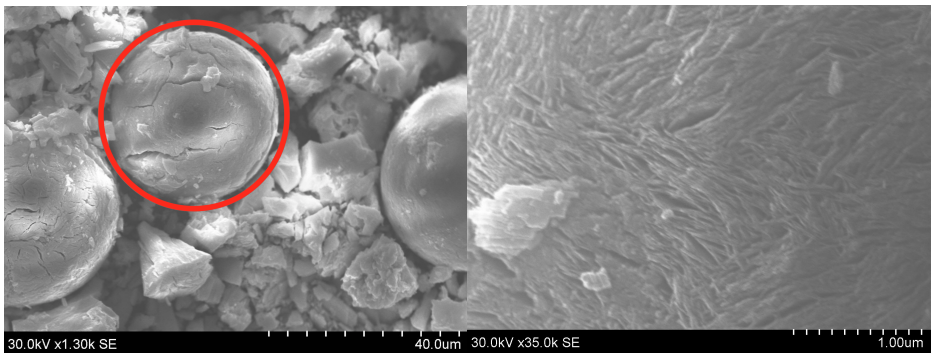

(a) **(b)**

Figure 4.10: SEM of CZW-Cu sample, where (a) shows spherical particles observed and (b) shows the surface of the circled spherical particle.

EDS image of this sample was also performed and shown in Figure 4.11. An arbitrary surface of a spherical particle (image (a) to the left) was used to do an elemental mapping (b). From this image, we can see that certain areas of the surface has stronger signals of specific elements than others. Although the signals in general were homogeneously distributed, as shown in Figure 4.12.

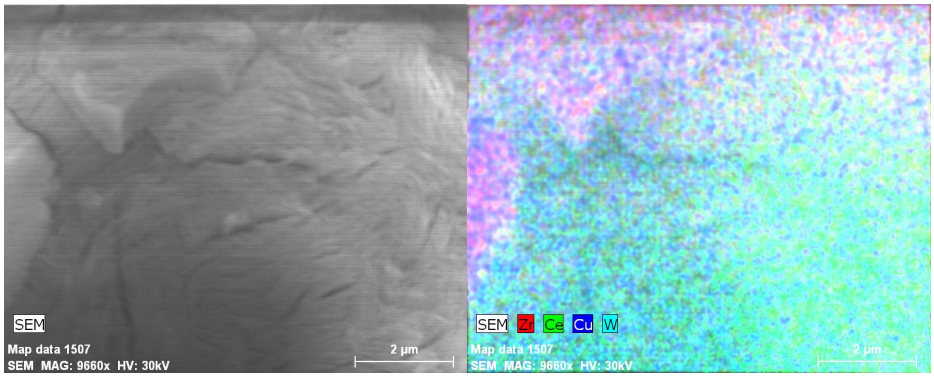

(a) SEM picture with area of interest **(b)** Elemental mapping of (a)

Figure 4.11: EDS image of CZW-Cu sample. (a) is the surface of a arbitrary spherical particle and (b) is the elemental mapping with 4 additional filters overlapping the original image. The 4 different filters are the elemental mapping obtained by EDS for the elements Ce, Zr, W and Cu.

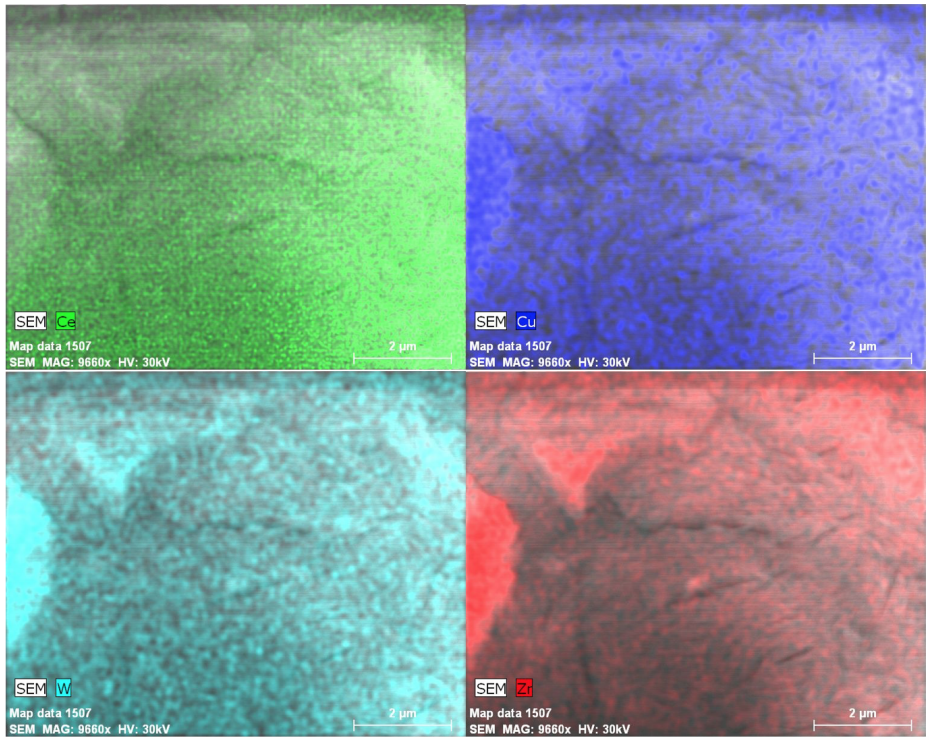

Figure 4.12: The 4 separate signals from the different elements from the same image (a) in Figure 4.11. Where each element is represented by their own color.

4.6.3 CZW-CuImpr

Figure 4.13 shows the SEM images taken from the CZW-CuImpr sample. Most of the particles observed were in different shapes and sizes. No spherical particles were observed in this catalyst contrary to the other two catalysts. The image to the right (b) shows a close-up of an arbitrary particle and shows some distribution of smaller particles on the surface.

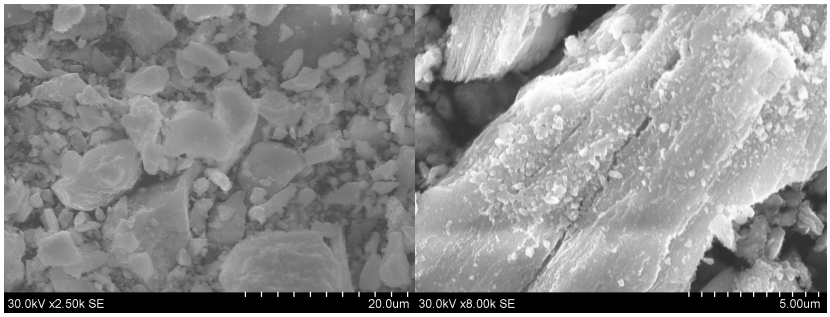

(a) randomly selected area **(b)** surface of an arbitrary particle

Figure 4.13: SEM image of CZW-CuImpr sample

EDS was also performed on this sample to determine the surface species and distribution. The images in Figure 4.14 shows a randomly selected surface where tiny particles are clearly visible on the surface. To further determine the specific species, an elemental mapping of the selected area was performed and shown in (b). From this image we can clearly see that some of the visible particles on the surface indicate copper, while the distribution of other elements are rather homogeneous. Figure 4.15 shows the separate signal for Cu, where the white particles previously shown in the SEM image now clearly indicates Cu. This confirms the speculation of dispersed Cu, resulting in reduced intensity in the XRD diffractogram.

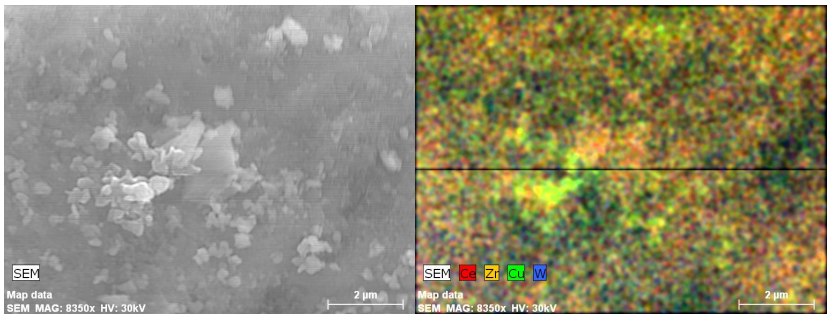

(a) Selected surface for EDS **(b)** Elemental mapping of selected area

Figure 4.14: EDS image of CZW-CuImpr sample

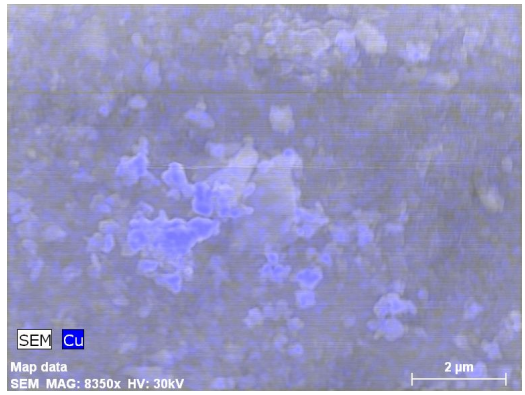

Figure 4.15: Cu signal for the selected area, indicating clearly Cu particles on the surface of the chosen particle.

4.7 Activity test

The catalytic activity plot of CZW is shown in Figure 4.16. Three different temperatures were used to test for the catalytic performance, and these temperatures were 150, 200 and 250 °C. Only NO and NH_3 is shown in the plot for clearer comparison, but a more comprehensive plot can be found in Appendix D. The important area to note is the changes occurring around 170, 260 and 410 minutes. These were the times where NH_3 was fed to the system, resulting in the SCR reduction of NO.

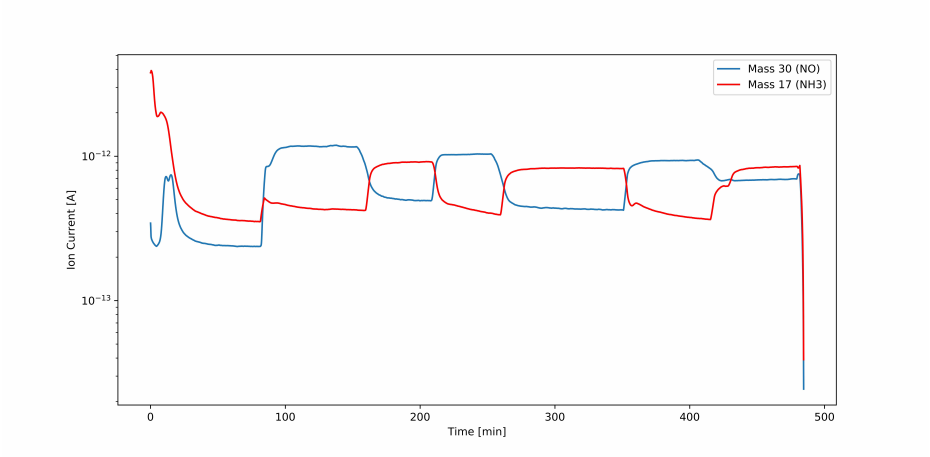

Figure 4.16: The SCR activity measurement of the CZW catalyst. Where the change after the 170 (250 °C), 260 (200 °C) and 410 (150 °C) minute mark is of interest, where all the reactants are present and SCR occurs (where the blue line decreases and red line increases). 10% O_2 was fed simultaneously with NO and therefore not shown in the plot.

Figure 4.17 shows the catalytic activity test for the CZW-Cu catalyst. The same three temperatures were utilized for this test; 150, 200 and 250 °C. A more comprehensive plot can be found in Appendix D. The important time aspects to note in this test is occurring around the 150 (250 °C SCR reaction), 250 (200 °C SCR reaction) and 400 (150 °C SCR reaction) minute mark.

The catalytic activity of the CZW-CuImpr catalyst i shown in Figure 4.18. This catalyst was tested with the similar parameter as the previously mentioned catalysts. A more comprehensive plot can be found in Appendix D For this catalyst, the SCR reactions occurred around 180, 280 and 350 minute mark. The SCR reactions for the catalyst were tested with a reaction temperature of 250, 200 and 150 °C respectively.

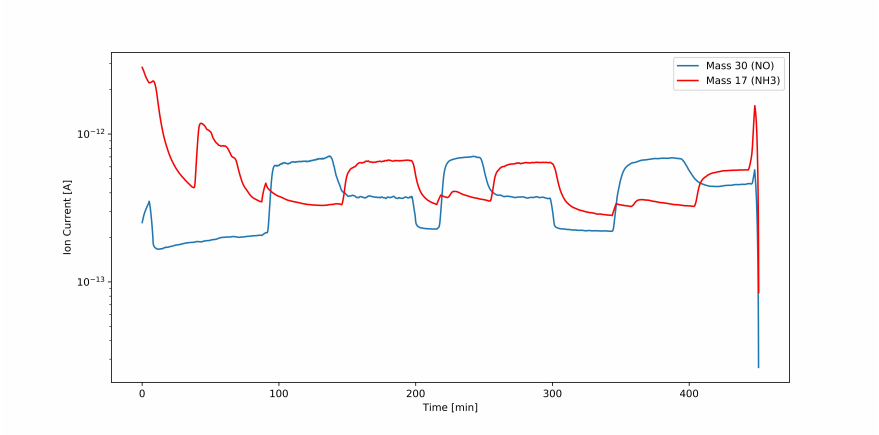

Figure 4.17: The first SCR reaction occurred around the 150 minute mark, with a reaction temperature of 250 °C. Followed by 200 and 150 °C occurring at 250 and 400 minute mark respectively. 10% O_2 was fed simultaneously with NO and therefore not shown in the plot.

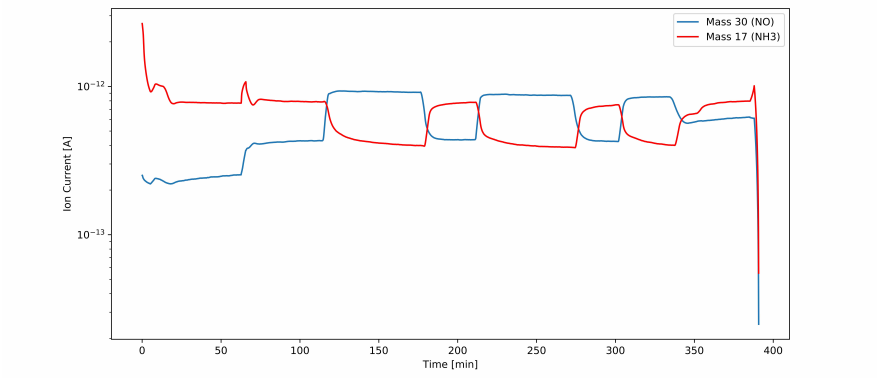

Figure 4.18: SCR reactions for the catalyst were tested for temperatures of 250, 200 and 150 °C occurring around 180, 280 and 350 minute mark. 10% O_2 was fed simultaneously with NO and therefore not shown in the plot.

The NO conversion and NO concentration at steady-state SCR reaction for the three reaction temperatures for all catalysts are presented in Table 4.4. The numbers are based on the average values taken from last 20 minutes where the steady-state is established.

The catalyst with the highest NO conversion was found to be the CZW-Cu catalyst, for all the temperatures tested. Between CZW and CZW-CuImpr, the latter catalyst showed a higher catalytic activity at lower temperature, but at the higher temperatures (200-250 °C) they exhibited close to equal conversions.

Figure 4.19 shows the NO conversion for all the catalysts for the three reaction temperatures. It can be seen that the CZW-Cu catalyst shows higher activity over the different temperatures, whereas the two others are less active at the lower temperature.

Table 4.4: Concentration of NO at SCR steady-state and conversion of NO at the three temperatures tested for all samples. The concentration was calculated by correlating the ion current at steady-state SCR of NO with the linear correlation obtained from the calibration of NO.

Sample	Temperature °C	Concentration at steady-state (ppm)	NO conversion (%)
CZW-Cu	150	150	75.0
	200	124	79.3
	250	124	79.3
CZW-CuImpr	150	199	66.8
	200	143	76.2
	250	145	75.8
CZW	150	229	61.8
	200	143	76.2
	250	167	72.2

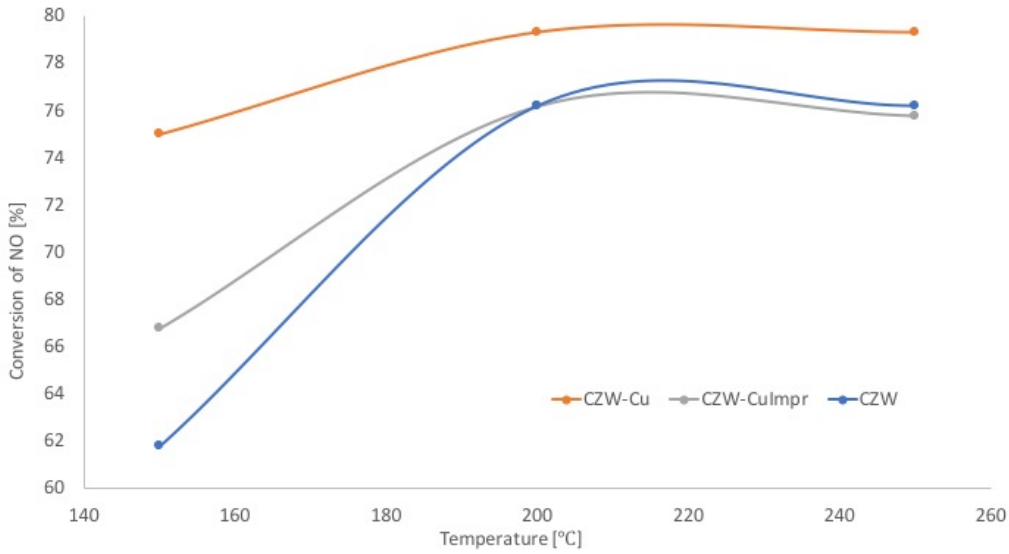

Figure 4.19: Comparison of the NO conversion for the three catalysts at the different reaction temperatures.

4.8 Short summary of results and discussion

The CZW catalyst had the lowest activity of all the catalyst at a reaction temperature of $150\,^{\circ}\mathrm{C}$, which is unexpected because of the higher surface area compared to the CZW-CuImpr catalyst. The two catalysts had similar pore size (6.4 and 6.2 nm respectively), while the BET surface was 62 and 42 m^2 g^{-1} for CZW and CZW-CuImpr respectively. One would expect the CZW to have a higher catalytic activity due to higher surface area, leading to the possibility of more active sites. One possible explanation of lower activity on CZW compared to CZW-CuImpr could be the Cu on CZW-CuImpr, since the addition of Cu seems to be the one factor that separated the two catalysts distinctively. The addition of small amounts of Cu was reported to increase the SCR activity, but does not explain why the activity of both catalysts were almost identical at the higher reaction temperatures. When one would expect the CZW-CuImpr to have better activity at the higher reaction temperatures as well. Another explanation could be that the activity of the CZW-CuImpr catalyst should have been higher, but due to the undesired ratio (0.7:1:0.25 for Ce, Zr and W) have changed the morphology and surface properties of the catalyst, which can be confirmed by the XRD, SEM and EDS images captured. Where it was clear that spherical particles were observed in the CZW and CZW-Cu sample, but not in the CZW-CuImpr sample. Cu particles were also observed on the catalyst surface of CZW-CuImpr, which could have occupied active sites or sealed pores, resulting in the similar activity to CZW at higher temperature.

Since the highest NO conversion was found in the CZW-Cu sample, it can be speculated that the addition of Cu improved the SCR activity. Even though both CZW and CZW-CuImpr had similar conversion it was clear that a SCR temperature above $150\,^{\circ}\mathrm{C}$ was more favorable for these two catalysts, while the CZW-Cu catalyst exhibited more stable SCR activity over the entire temperature range. When comparing CZW to CZW-Cu, the only distinguishable difference is the addition of Cu, because both catalysts were synthesized by the hydrothermal method. The addition of Cu also gave a greater surface area, better thermal stability and better catalytic activity across the reaction temperatures. From SEM and EDS it was hard to differentiate the two catalysts, as both catalysts had similar surface rifts and spherical particles. The addition of Cu also indicated active redox reactions at the active SCR temperatures, which can be one of the reasons why the activity of CZW-Cu was greater.

Comparing the CZW-Cu and CZW-CuImpr catalysts, both had the addition of roughly 3% Cu, but were synthesized through two different methods. The hydrothermal method and the impregnation of Cu on a CZW-support resulted in different morphology and surface characteristics for the two catalyst as seen in SEM/EDS and TPR. The undesired atomic ratio can have resulted in a decreased performance for the SCR reaction for the CZW-CuImpr catalyst, but needs further testing to confirm.

Chapter 5

Conclusion

Three catalyst based on Ce, Zr and W was successfully synthesized by the hydrothermal and dry impregnation method. The aim of synthesizing catalyst with the atomic ratio of 1:1:0.25 for Ce, Zr and W respectively was achieved by the CZW and CZW-Cu catalyst. The CZW-CuImpr catalyst achieved a ratio of 0.75:1:0.25 due to the support, which also contained the similar atomic ratio. Both Cu containing catalysts achieved a 3 mass percent Cu loading, which was confirmed by XRF, XRD and S(T)EM. All catalysts showed thermal stability over a wide temperature range up to the calcination temperature at $550\,^{\circ}\mathrm{C}$.

BET analysis found the surface area of the catalysts to be 62, 76 and 42 $m^2\ g^{-1}$ for CZW, CZW-Cu and CZW-CuImpr respectively. The average pore size was also found to be 6.4, 3.6 and 6.2 nm respectively. The pore volume was highest for the CZW catalyst, with 0.098 $cm^3\ g^{-1}$, while lowest for the CZW-Cu sample with only 0.075 $cm^3\ g^{-1}$.

Based on the finding and discussions, the CZW-Cu catalyst was the most promising catalyst for low-temperature SCR reaction, with its stable catalytic activity over a wider range of temperature. The addition of Cu also seemed to promote the SCR reaction and thermal stability of the catalyst. The hydrothermal synthesis method was also better for the catalyst structure and surface properties, which led to a higher surface area.

Chapter 6

Further work

For future work on this project a good starting point would be to reproduce the CZW-CuImpr catalyst with the desired atomic ratio on Ce, Zr and W, then have the addition of Cu. This could quickly determine if the hydrothermal method is inferior to the impregnation method or opposite.

Another aspect worth pursuing is the ratio of Ce and Zr in the catalyst. By synthesizing different catalysts with varying ratio between Ce/Zr to determine the optimal ratio between these metals. As it seem to have an impact on the SCR activity it can be worth investigating.

Further variation of the amount of Cu added to the catalyst can also be explored to see whether a higher loading of Cu has a better effect on SCR activity than the current one.

A more comprehensive TPR study could also be performed to determine the effects of the redox reaction on the SCR activity.

More sophisticated catalytic activity can be done, in order to obtain more accurate measurements that is easier to distinguish.

Bibliography

[1] IMO. IMO regulations to reduce air pollution from ships and the review of fuel oil availability, 2016. Available at: http://www.imo.org/en/MediaCentre/HotTopics/GHG/Documents/sulphurlimitsFAQ{_}20-09-2016.pdf.

[2] Haifeng Wang. The end of the era of heavy fuel oil in maritime shipping, 2014. Available at: https://www.theicct.org/blogs/staff/end-era-heavy-fuel-oil-maritime-shipping.

[3] Enerdata. Natural Gas Production, 2017. Available at: https://yearbook.enerdata.net/natural-gas/world-natural-gas-production-statistics.html.

[4] Ping Ning, Zhongxian Song, Hao Li, Qiulin Zhang, Xin Liu, Jinhui Zhang, Xiaosu Tang, and Zhenzhen Huang. Selective catalytic reduction of NO with NH3 over CeO2ZrO2WO3 catalysts prepared by different methods. *Applied Surface Science*, 332(Supplement C):130–137, 2015.

[5] Zhongxian Song, Ping Ning, Qiulin Zhang, Hao Li, Jinhui Zhang, Yancai Wang, Xin Liu, and Zhenzhen Huang. Activity and hydrothermal stability of CeO2ZrO2WO3 for the selective catalytic reduction of NOx with NH3. *Journal of Environmental Sciences*, 42(Supplement C):168–177, 2016.

[6] Zhongxian Song, Liangtao Yin, Qiulin Zhang, Ping Ning, Yankang Duan, Jing Wang, Xin Liu, Kaixian Long, and Zhenzhen Huang. Relationship between the WO3 states and reaction pathway over CeO2-ZrO2-WO3 catalysts for selective catalytic reduction of NO with NH3. *Molecular Catalysis*, 437(Supplement C):95–104, 2017.

[7] Miljødirektoratet. NOx, 2017. Available at: http://www.miljostatus.no/tema/luftforurensning/sur-nedbor/nitrogenoksid-nox/.

[8] Clean Air Technology Center. Nitrogen Oxides (NOx) Why and how they are controlled. Technical report, Clean Air Technology Center, 1999. Available at: https://www3.epa.gov/ttncatc1/dir1/fnoxdoc.pdf.

[9] Zhong-xian SONG, Qiu-lin ZHANG, Jin-hui ZHANG, Ping NING, Hao LI, Yan-cai WANG, Ming-zhi WANG, and Yan-kang DUAN. Effect of WO3 content on the catalytic activity of CeO2-ZrO2-WO3 for selective catalytic reduction of NO with NH3. *Journal of Fuel Chemistry and Technology*, 43(6):701–707, jun 2015.

[10] Quan Xu, Wenjing Yang, Shitong Cui, Jason Street, and Yan Luo. Sulfur resistance of Ce-Mn/TiO 2 catalysts for low-temperature NH 3 SCR. *Royal Society Open Science*, 5(3):171846, mar 2018.

[11] Manfred Koebel, Giuseppe Madia, and Martin Elsener. Selective catalytic reduction of NO and NO2 at low temperatures. *Catalysis Today*, 73(3):239–247, 2002.

[12] Wenchao Yu, Xiaodong Wu, Zhichun Si, and Duan Weng. Influences of impregnation procedure on the SCR activity and alkali resistance of V2O5WO3/TiO2 catalyst. *Applied Surface Science*, 283:209–214, 2013.

[13] Malcolm Yates, Juan Antonio Martín, M Ángeles Martín-Luengo, Silvia Suárez, and Jesús Blanco. N2O formation in the ammonia oxidation and in the SCR process with V2O5-WO3 catalysts. *Catalysis Today*, 107-108:120–125, oct 2005.

[14] Fudong Liu, Kiyotaka Asakura, Hong He, Wenpo Shan, Xiaoyan Shi, and Changbin Zhang. Influence of sulfation on iron titanate catalyst for the selective catalytic reduction of NOx with NH3. *Applied Catalysis B: Environmental*, 103(3):369–377, 2011.

[15] Liang Chen, Junhua Li, and Maofa Ge. DRIFT Study on CeriumTungsten/Titiania Catalyst for Selective Catalytic Reduction of NO x with NH 3. *Environmental Science & Technology*, 44(24):9590–9596, dec 2010.

[16] Zhixiang Zhang, Mingxia Chen, Zhi Jiang, and Wenfeng Shangguan. Low-temperature selective catalytic reduction of NO with propylene in excess oxygen over the Pt/ZSM-5 catalyst. *Journal of Hazardous Materials*, 193:330–334, 2011.

[17] Hirofumi Ohtsuka and Takeshi Tabata. Roles of palladium and platinum in the selective catalytic reduction of nitrogen oxides by methane on palladiumplatinum-loaded sulfated zirconia. *Applied Catalysis B: Environmental*, 29(3):177–183, 2001.

[18] Erol Seker and Erdogan Gulari. Single step solgel made gold on alumina catalyst for selective reduction of NOx under oxidizing conditions: effect of gold precursor and reaction conditions. *Applied Catalysis A: General*, 232(1):203–217, 2002.

[19] Isabella Nova and Enrico Tronconi. *Urea-SCR Technology for deNOx after Treatment of Diesel Exhausts*. Springer Berlin Heidelberg, 2014.

[20] Wenpo Shan, Fudong Liu, Hong He, Xiaoyan Shi, and Changbin Zhang. Novel cerium-tungsten mixed oxide catalyst for the selective catalytic reduction of NOx with NH3. *Chem. Commun.*, 47(28):8046–8048, 2011.

[21] G W Graham, H.W. Jen, R W McCabe, A M Straccia, and L P Haack. Characterization of model automotive exhaust catalysts: Pd on Zrrich ceria–zirconia supports. *Catalysis Letters*, 67(2):99–105, jul 2000.

[22] Masaaki Haneda, Tomoko Morita, Yukinori Nagao, Yoshiaki Kintaichi, and Hideaki Hamada. CeO2-ZrO2 binary oxides for NOx removal by sorption. *Phys. Chem. Chem. Phys.*, 3(21):4696–4700, 2001.

[23] Zhiming Liu, Yuxian Liu, Yuan Li, Hang Su, and Lingling Ma. WO3 promoted MnZr mixed oxide catalyst for the selective catalytic reduction of NOx with NH3. *Chemical Engineering Journal*, 283:1044–1050, 2016.

[24] Ye Li, Hao Cheng, Deyi Li, Yongsheng Qin, Yuming Xie, and Shudong Wang. WO3/CeO2-ZrO2, a promising catalyst for selective catalytic reduction (SCR) of NOx with NH3 in diesel exhaust. *Chemical Communications*, (12):1470, 2008.

[25] Li Xiaowei, Shen Mingmin, Hong Xi, Zhu Haiyang, Gao Fei, Kong Yan, Dong Lin, and Chen Yi. Dispersion and Reduction of Copper Oxide Supported on WO 3 -Modified Ce 0.5 Zr 0.5 O 2 Solid Solution. *The Journal of Physical Chemistry B*, 109(9):3949–3955, mar 2005.

[26] Yuanshan Li, Haidi Xu, Xi Feng, Shuang Liu, and Yaoqiang Chen. The effective promotion of trace amount of Cu on Ce/WO 3 -ZrO 2 -TiO 2 monolithic catalyst for the low-temperature NH 3 -SCR of NO x. *The Canadian Journal of Chemical Engineering*, 96(5):1168–1175, may 2018.

[27] Guangpeng Yang, Jingyu Ran, Xuesen Du, Xiangmin Wang, Yanrong Chen, and Li Zhang. Different copper species as active sites for NH3-SCR reaction over Cu-SAPO-34 catalyst and reaction pathways: A periodic DFT study. *Microporous and Mesoporous Materials*, 266:223–231, 2018.

[28] George W. Morey. Hydrothermal Synthesis. *Journal of the American Ceramic Society*, 36(9):279–285, sep 1953.

[29] Albrecht Rabenau. The Role of Hydrothermal Synthesis in Preparative Chemistry. *Angewandte Chemie International Edition in English*, 24(12):1026–1040, dec 1985.

[30] Pablo Cubillas and Michael W. Anderson. Synthesis Mechanism: Crystal Growth and Nucleation. In *Zeolites and Catalysis*, pages 1–55. Wiley-VCH Verlag GmbH & Co. KGaA, Weinheim, Germany, jun 2010.

[31] Helmut Knözinger and Karl Kochloefl. Heterogeneous Catalysis and Solid Catalysts. In *Ullmann's Encyclopedia of Industrial Chemistry*. Wiley-VCH Verlag GmbH & Co. KGaA, Weinheim, Germany, jan 2003.

[32] Carlo Perego and Pierluigi Villa. Catalyst preparation methods. *Catalysis Today*, 34(3-4):281–305, feb 1997.

[33] Eric Marceau, Xavier Carrier, and Michel Che. Impregnation and Drying. In *Synthesis of Solid Catalysts*, pages 59–82. Wiley-VCH Verlag GmbH & Co. KGaA, Weinheim, Germany, 2009.

[34] Dr. I Chorkendorff and J. W. Niemantsverdriet. Catalyst Characterization. In *Concepts of Modern Catalysis and Kinetics*, pages 129–166. Wiley-VCH Verlag GmbH & Co. KGaA, Weinheim, FRG, jan 2005.

[35] Yuriy P. Gnatenko. X-ray Diffraction, 2017. Available at: `https://www.researchgate.net/profile/Yuriy_Gnatenko2/post/How_to_determine_crystal_size_and_coating_thickness_from_XRD_analysis_results_by_using_Braggs_Law`.

[36] Peter Brouwer. *Theory of XRF*. PANalytical B.V., Almelo, 3rd edition, 2010.

[37] G A Jeffery. Elements of x-ray diffraction (Cullity, B. D.). *Journal of Chemical Education*, 34(4):A178, apr 1957.

[38] Stephen Brunauer, P. H. Emmett, and Edward Teller. Adsorption of Gases in Multimolecular Layers. *Journal of the American Chemical Society*, 60(2):309–319, feb 1938.

[39] I. Chorkendorff and J. W. Niemantsverdriet. *Concepts of Modern Catalysis and Kinetics*. Wiley-VCH Verlag GmbH & Co. KGaA, Weinheim, FRG, oct 2003.

[40] K. S. W. Sing. Reporting physisorption data for gas/solid systems with special reference to the determination of surface area and porosity (Provisional). *Pure and Applied Chemistry*, 54(11):2201–2218, jan 1982.

[41] Robert M. Fitch. Principles of colloid and surface chemistry, by Paul C. Hiemenz, Marcel Dekker, New York, 1977, 516 pp. No Price given. *Journal of Polymer Science: Polymer Letters Edition*, 22(9):508–509, sep 1984.

[42] Elliott P. Barrett, Leslie G. Joyner, and Paul P. Halenda. The Determination of Pore Volume and Area Distributions in Porous Substances. I. Computations from Nitrogen Isotherms. *Journal of the American Chemical Society*, 73(1):373–380, jan 1951.

[43] G. W. H. Höhne, W. F. Hemminger, and H.-J. Flammersheim. *Differential Scanning Calorimetry*. Springer Berlin Heidelberg, Berlin, Heidelberg, 2003.

[44] Julian Heath, Nick (Spectroscopy Taylor, and Separations EKB Series). Energy Dispersive Spectroscopy, 2015.

[45] William Reusch. Mass Spectrometry, 2013.

[46] NIST Mass Spec Data Center and S.E Stein, director. *Mass spectra*. NIST Chemistry WebBook, NIST Standard Reference Database Number 69, Eds. P.J. Linstrom and W.G. Mallard, National Institute of Standards and Technology, Gaithersburg MD, 20899. doi:10.18434/T4D303, (retrieved march 11, 2018).

[47] Pradyot Patnaik. *Dean's Analytical Chemistry Handbook, Second Edition*. McGRAW-HILL: New York, Chicago, San Francisco, Lisbon, London, Madrid, Mexico City, Milan, New Delhi, San Juan, Seoul, Singapore, Sydney, Toronto, second edi edition, 2004.

[48] R. Moreno-Tost, J. Santamaría-González, P. Maireles-Torres, F. Rodríguez-Castellón, and A. Jiménez-López. Selective catalytic reduction of NO by ammonia at low temperatures on catalysts based on copper oxide supported on a zirconium-doped mesoporous silica. *Catalysis Letters*, 82(3-4):205–212, 2002.

[49] Lj Kundakovic and M Flytzani-Stephanopoulos. Reduction characteristics of copper oxide in cerium and zirconium oxide systems. *Applied Catalysis A: General*, 171(1):13–29, jun 1998.

[50] J Sárkány, J L D'Itri, and W M H Sachtler. Redox chemistry in excessively ion-exchanged Cu/Na-ZSM-5. *Catalysis Letters*, 16(3):241–249, 1992.

Appendix A

Sample weight used in characterization

Characterization method	Catalyst used [mg] CZW	CZW-Cu	CZW-CuImpr
XRD	Not measured	Not measured	Not measured
XRF	200	200	180
BET	110	453	257
TGA	16	20	21
TPR	100	100	100

Appendix B

XRD diffractogram

B.1 CZW-Cu

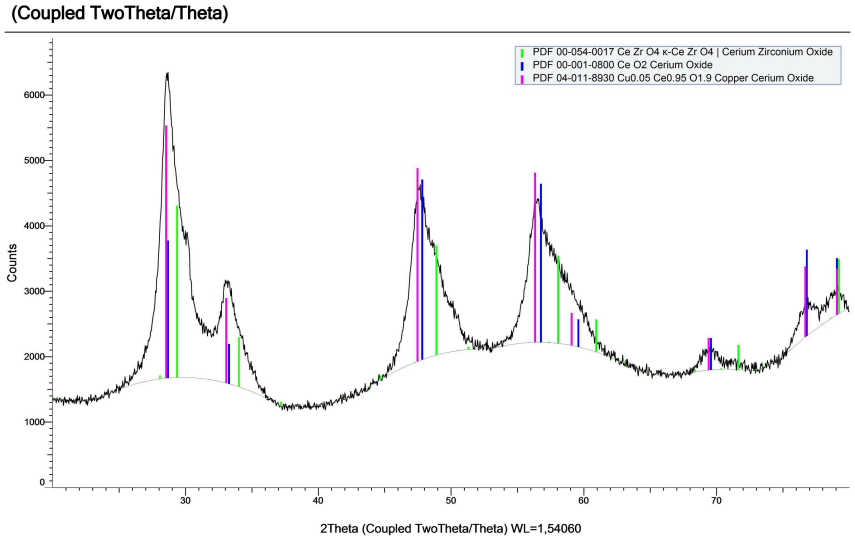

B.2 CZW-CuImpr

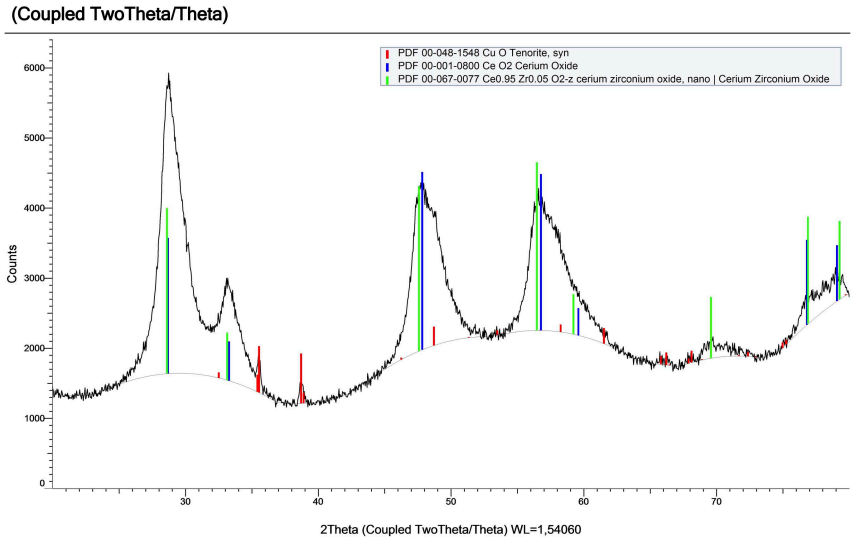

Appendix C

BET Data

C.1 CZW

Full Report Set

Sample: Zr,Cr,W
Operator: KIN
Submitter:
File: C:\Users\labuser\Desktop\BET data from ...\000-030.SMP

Started:	12.11.2017 15:44:13	Analysis Adsorptive:	N2
Completed:	12.11.2017 21:29:37	Analysis Bath Temp.:	-195,800 °C
Report Time:	12.06.2018 11:43:50	Thermal Correction:	No
Sample Mass:	0,1105 g	Warm Free Space:	11,4373 cm³ Measured
Cold Free Space:	33,8073 cm³	Equilibration Interval:	5 s
Low Pressure Dose:	None	Sample Density:	1,000 g/cm³
Automatic Degas:	No		

Summary Report

Surface Area

Single point surface area at p/p° = 0,300013699: 61,7504 m²/g

BET Surface Area: 65,2321 m²/g

Pore Volume

Single point adsorption total pore volume of pores less than 3 695,374 Å width at p/p° = 0,994757172: 0,109718 cm³/g

BJH Adsorption cumulative volume of pores between 17,000 Å and 3 000,000 Å width: 0,105507 cm³/g

BJH Desorption cumulative volume of pores between 17,000 Å and 3 000,000 Å width: 0,108586 cm³/g

Pore Size

Adsorption average pore diameter (4V/A by BET): 67,2784 Å

BJH Adsorption average pore width (4V/A): 82,126 Å

BJH Desorption average pore width (4V/A): 76,145 Å

Sample: Zr,Cr,W
Operator: KIN
Submitter:
File: C:\Users\labuser\Desktop\BET data from ...\000-030.SMP

Started: 12.11.2017 15:44:13
Completed: 12.11.2017 21:29:37
Report Time: 12.06.2018 11:43:50
Sample Mass: 0,1105 g
Cold Free Space: 33,8073 cm³
Low Pressure Dose: None
Automatic Degas: No

Analysis Adsorptive: N2
Analysis Bath Temp.: -195,800 °C
Thermal Correction: No
Warm Free Space: 11,4373 cm³ Measured
Equilibration Interval: 5 s
Sample Density: 1,000 g/cm³

Isotherm Tabular Report

Relative Pressure (p/p°)	Absolute Pressure (mmHg)	Quantity Adsorbed (mmol/g)	Elapsed Time (h:min)	Saturation Pressure (mmHg)
			00:39	745.495544
0.010101428	7.546011	0.50707	00:44	747.024170
0.030560820	22.838507	0.57920	00:46	747.313293
0.065115481	48.667412	0.64775	00:48	747.401550
0.079275443	59.258911	0.66956	00:50	747.506531
0.099657988	74.493355	0.69779	00:52	747.490051
0.119804989	89.547882	0.72304	00:55	747.447021
0.140131208	104.738251	0.74697	00:57	747.429871
0.160360505	119.856255	0.76954	00:59	747.417542
0.180558480	134.938568	0.79083	01:01	747.339966
0.200469451	149.803146	0.81127	01:02	747.261719
0.249137140	186.151031	0.85763	01:04	747.182983
0.300013699	224.164032	0.90424	01:06	747.179321
0.350012083	261.497009	0.94894	01:08	747.108521
0.398690626	297.836182	0.99189	01:09	747.035828
0.448364567	334.936432	1.03779	01:11	747.018066
0.498328066	372.232086	1.08601	01:13	746.961914
0.548070547	409.352600	1.13785	01:15	746.897644
0.597783783	446.464691	1.19526	01:17	746.866516
0.647525014	483.597046	1.26082	01:18	746.839172
0.697227187	520.674744	1.33796	01:20	746.779175
0.746829491	557.646240	1.43234	01:23	746.684814
0.795927271	594.157959	1.55837	01:26	746.497803
0.818844997	611.273438	1.63239	01:28	746.506897
0.847300269	632.431458	1.74661	01:31	746.407715
0.872302100	650.902893	1.87304	01:34	746.189758
0.896556367	668.920410	2.03562	01:38	746.099670
0.922050700	687.707947	2.24010	01:41	745.846130
0.944996524	704.526978	2.49859	01:47	745.533936
0.971037377	723.617065	2.82737	01:52	745.200012
0.979726255	729.902100	2.93924	01:55	745.006165
0.988203806	735.990479	3.06839	01:59	744.776001
0.994757172	740.707581	3.16462	02:01	744.611450
0.975317620	726.124207	3.09891	02:03	744.500244
0.961483305	715.672974	3.01198	02:06	744.342590
0.941050567	700.263733	2.86456	02:09	744.129761
0.926650955	689.388550	2.75433	02:12	743.957092
0.903341682	671.824097	2.56927	02:16	743.709839
0.879012561	653.445190	2.36323	02:20	743.385498
0.852623376	633.628540	2.15727	02:24	743.151733
0.828556534	615.497803	1.98869	02:28	742.855530
0.802954897	596.325500	1.83639	02:31	742.663757
0.754389419	560.088928	1.61669	02:35	742.440063

Sample: Zr,Cr,W
Operator: KIN
Submitter:
File: C:\Users\labuser\Desktop\BET data from ...\000-030.SMP

Started: 12.11.2017 15:44:13
Completed: 12.11.2017 21:29:37
Report Time: 12.06.2018 11:43:50
Sample Mass: 0,1105 g
Cold Free Space: 33,8073 cm³
Low Pressure Dose: None
Automatic Degas: No

Analysis Adsorptive: N2
Analysis Bath Temp.: -195,800 °C
Thermal Correction: No
Warm Free Space: 11,4373 cm³ Measured
Equilibration Interval: 5 s
Sample Density: 1,000 g/cm³

Isotherm Tabular Report

Relative Pressure (p/p°)	Absolute Pressure (mmHg)	Quantity Adsorbed (mmol/g)	Elapsed Time (h:min)	Saturation Pressure (mmHg)
0.704157285	522.666504	1.45914	02:39	742.258179
0.654518557	485.679535	1.34811	02:41	742.040894
0.603843812	447.944305	1.26142	02:43	741.821472
0.552985710	410.158081	1.19004	02:45	741.715515
0.502372735	372.564606	1.12989	02:47	741.609924
0.453407565	336.189423	1.05784	02:49	741.472900
0.400812562	297.121124	0.98999	02:51	741.296936
0.351190010	260.292694	0.94103	02:53	741.173401
0.301781467	223.633163	0.89655	02:55	741.043396
0.251323939	186.215500	0.85058	02:56	740.938171
0.201080302	148.942551	0.80195	02:58	740.711792
0.140971256	104.406372	0.73876	03:00	740.621704

Sample: Zr,Cr,W
Operator: KIN
Submitter:
File: C:\Users\labuser\Desktop\BET data from ...\000-030.SMP

Started:	12.11.2017 15:44:13	Analysis Adsorptive:	N2
Completed:	12.11.2017 21:29:37	Analysis Bath Temp.:	-195,800 °C
Report Time:	12.06.2018 11:43:50	Thermal Correction:	No
Sample Mass:	0,1105 g	Warm Free Space:	11,4373 cm³ Measured
Cold Free Space:	33,8073 cm³	Equilibration Interval:	5 s
Low Pressure Dose:	None	Sample Density:	1,000 g/cm³
Automatic Degas:	No		

Isotherm Linear Plot

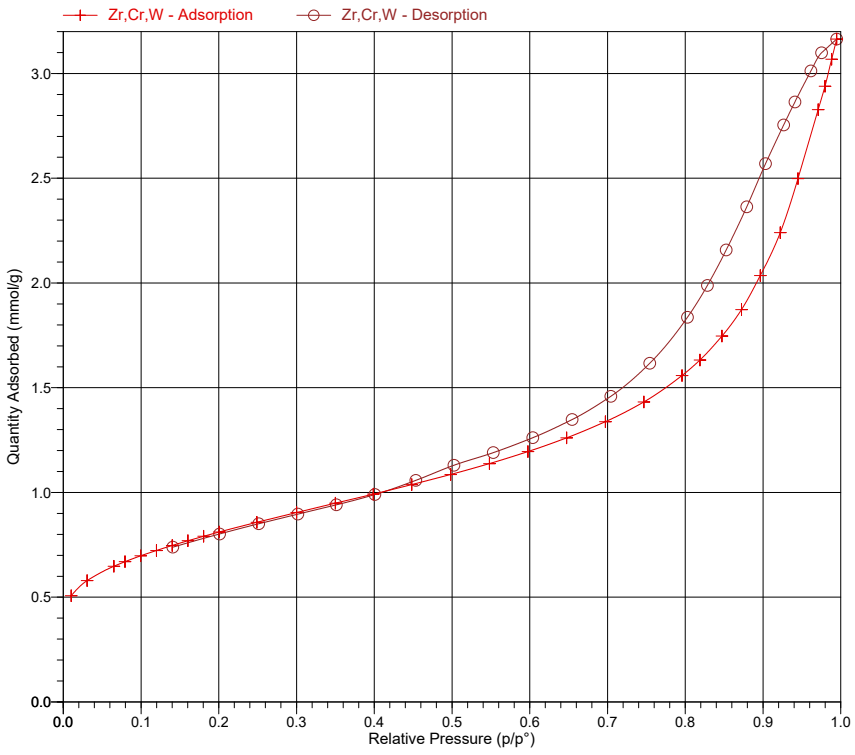

Sample: Zr,Cr,W
Operator: KIN
Submitter:
File: C:\Users\labuser\Desktop\BET data from ...\000-030.SMP

Started:	12.11.2017 15:44:13	Analysis Adsorptive:	N2
Completed:	12.11.2017 21:29:37	Analysis Bath Temp.:	-195,800 °C
Report Time:	12.06.2018 11:43:50	Thermal Correction:	No
Sample Mass:	0,1105 g	Warm Free Space:	11,4373 cm³ Measured
Cold Free Space:	33,8073 cm³	Equilibration Interval:	5 s
Low Pressure Dose:	None	Sample Density:	1,000 g/cm³
Automatic Degas:	No		

BET Report

BET Surface Area: 65.2321 ± 0.1645 m²/g
Slope: 1.484985 ± 0.003735 g/mmol
Y-Intercept: 0.010585 ± 0.000516 g/mmol
C: 141.295106
Qm: 0,66864 mmol/g
Correlation Coefficient: 0.9999810
Molecular Cross-Sectional Area: 0.1620 nm²

Relative Pressure (p/p°)	Quantity Adsorbed (mmol/g)	1/[Q(p°/p - 1)]
0.065115481	0.64775	0.10753
0.079275443	0.66956	0.12859
0.099657988	0.69779	0.15863
0.119804989	0.72304	0.18825
0.140131208	0.74697	0.21817
0.160360505	0.76954	0.24818
0.180558480	0.79083	0.27862
0.200469451	0.81127	0.30906

Sample: Zr,Cr,W
Operator: KIN
Submitter:
File: C:\Users\labuser\Desktop\BET data from ...\000-030.SMP

Started:	12.11.2017 15:44:13	Analysis Adsorptive:	N2
Completed:	12.11.2017 21:29:37	Analysis Bath Temp.:	-195,800 °C
Report Time:	12.06.2018 11:43:50	Thermal Correction:	No
Sample Mass:	0,1105 g	Warm Free Space:	11,4373 cm³ Measured
Cold Free Space:	33,8073 cm³	Equilibration Interval:	5 s
Low Pressure Dose:	None	Sample Density:	1,000 g/cm³
Automatic Degas:	No		

BET Surface Area Plot

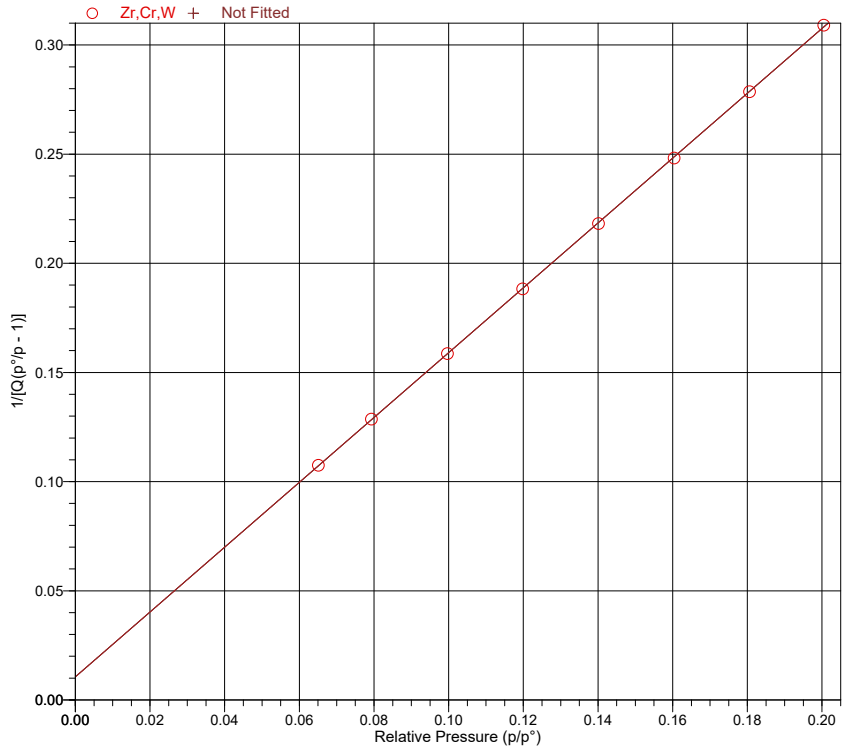

Sample: Zr,Cr,W
Operator: KIN
Submitter:
File: C:\Users\labuser\Desktop\BET data from ...\000-030.SMP

Started:	12.11.2017 15:44:13	Analysis Adsorptive:	N2
Completed:	12.11.2017 21:29:37	Analysis Bath Temp.:	-195,800 °C
Report Time:	12.06.2018 11:43:50	Thermal Correction:	No
Sample Mass:	0,1105 g	Warm Free Space:	11,4373 cm³ Measured
Cold Free Space:	33,8073 cm³	Equilibration Interval:	5 s
Low Pressure Dose:	None	Sample Density:	1,000 g/cm³
Automatic Degas:	No		

BJH Desorption dV/dw Pore Volume

Halsey : Faas Correction

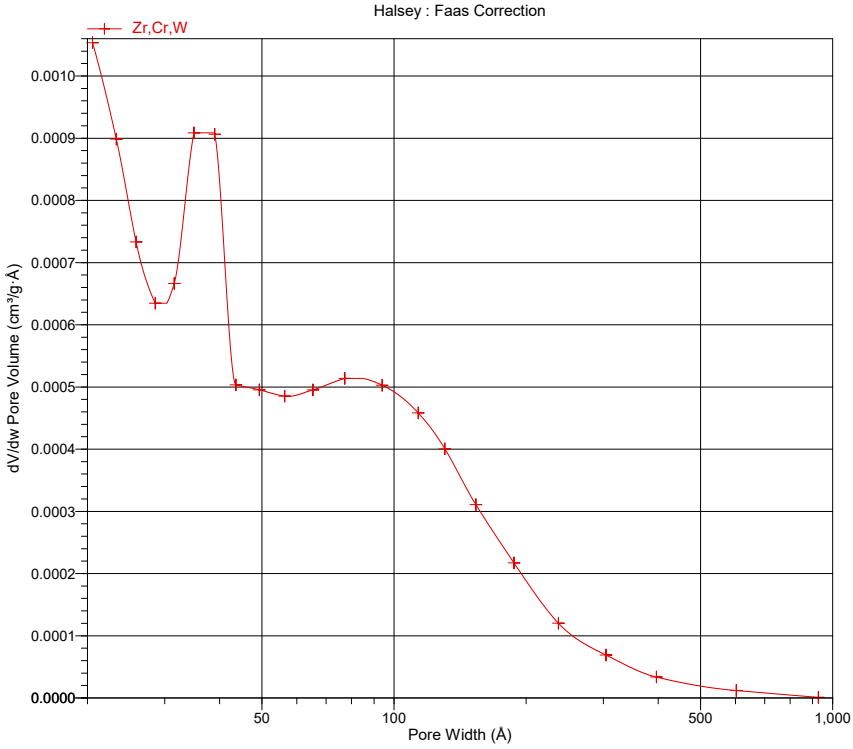

C.2 CZW-Cu

Full Report Set

Sample: template_180607
Operator: Kin
Submitter: Kin
File: C:\TriStar II 3020\d...\template_180607 - Cu_Port3.SMP

Started: 07.06.2018 14:30:30
Completed: 07.06.2018 18:10:07
Report Time: 12.06.2018 11:43:27
Sample Mass: 0,4530 g
Cold Free Space: 31,7370 cm³
Low Pressure Dose: None
Automatic Degas: No

Analysis Adsorptive: N2
Analysis Bath Temp.: -195,800 °C
Thermal Correction: No
Warm Free Space: 11,0346 cm³ Measured
Equilibration Interval: 5 s
Sample Density: 1,000 g/cm³

Summary Report

Surface Area

Single point surface area at p/p° = 0,298906275: 76,4342 m²/g

BET Surface Area: 77,8017 m²/g

Pore Volume

Single point adsorption total pore volume of pores less than 11,415 Å width at p/p° = 0,010000000: 0,021173 cm³/g

BJH Adsorption cumulative volume of pores between 17,000 Å and 3 000,000 Å width: 0,065987 cm³/g

BJH Desorption cumulative volume of pores between 17,000 Å and 3 000,000 Å width: 0,075134 cm³/g

Pore Size

Adsorption average pore diameter (4V/A by BET): 10,8854 Å

BJH Adsorption average pore width (4V/A): 33,845 Å

BJH Desorption average pore width (4V/A): 36,102 Å

Freundlich

Qm·C: 0,01017 ± 0.0092 mmol/g

m: 3.1455 ± 0.1635

Temkin

q·alpha/Qm: 1.655151 ± 0.126837 kJ/mol·(mmol/g)

A: 0.1503 ± 0.0686 mmHg

Sample: template_180607
Operator: Kin
Submitter: Kin
File: C:\TriStar II 3020\d...\template_180607 - Cu_Port3.SMP

Started: 07.06.2018 14:30:30
Completed: 07.06.2018 18:10:07
Report Time: 12.06.2018 11:43:27
Sample Mass: 0,4530 g
Cold Free Space: 31,7370 cm³
Low Pressure Dose: None
Automatic Degas: No

Analysis Adsorptive: N2
Analysis Bath Temp.: -195,800 °C
Thermal Correction: No
Warm Free Space: 11,0346 cm³ Measured
Equilibration Interval: 5 s
Sample Density: 1,000 g/cm³

Isotherm Tabular Report

Relative Pressure (p/p°)	Absolute Pressure (mmHg)	Quantity Adsorbed (mmol/g)	Elapsed Time (h:min)	Saturation Pressure (mmHg)
				740.000000
0.009840659	7.282088	0.60869	00:37	
0.031868074	23.582375	0.69254	00:42	
0.064043994	47.392555	0.76433	00:47	
0.077098120	57.052608	0.78826	00:50	
0.098807020	73.117195	0.82479	00:53	
0.118885783	87.975479	0.85626	00:57	
0.138857960	102.754890	0.88621	01:00	
0.158889430	117.578178	0.91534	01:04	
0.178911116	132.394226	0.94415	01:07	
0.199007189	147.265320	0.97278	01:10	
0.250058684	185.043427	1.04585	01:16	
0.298906275	221.190643	1.11749	01:20	
0.350216221	259.160004	1.19622	01:25	
0.397175639	293.909973	1.27143	01:30	
0.447071921	330.833221	1.35320	01:34	
0.496897352	367.704041	1.43563	01:39	
0.547118440	404.867645	1.51733	01:44	
0.597488733	442.141663	1.59452	01:48	
0.647803064	479.374268	1.66378	01:52	
0.698041431	516.550659	1.72347	01:56	
0.748081187	553.580078	1.77444	01:59	
0.797792919	590.366760	1.82034	02:02	
0.818826871	605.931885	1.83897	02:03	
0.848614832	627.974976	1.86572	02:05	
0.875057901	647.542847	1.88991	02:07	
0.899278878	665.466370	1.91284	02:09	
0.924016509	683.772217	1.93783	02:11	
0.948661103	702.009216	1.96619	02:14	
0.973284417	720.230469	2.00033	02:16	
0.980735325	725.744141	2.01322	02:18	
0.989776281	732.434448	2.02941	02:19	
0.994624122	736.021851	2.04188	02:21	
0.974671895	721.257202	2.02274	02:23	
0.940446596	695.930481	1.98324	02:25	
0.912081002	674.939941	1.95520	02:27	
0.901059785	666.784241	1.94491	02:29	
0.875588742	647.935669	1.92385	02:31	
0.850974088	629.720825	1.90479	02:32	
0.825716916	611.030518	1.88643	02:34	
0.801172040	592.867310	1.86964	02:35	
0.752124353	556.572021	1.83800	02:38	
0.701433914	519.061096	1.80573	02:40	

Sample: template_180607
Operator: Kin
Submitter: Kin
File: C:\TriStar II 3020\d...\template_180607 - Cu_Port3.SMP

Started: 07.06.2018 14:30:30
Completed: 07.06.2018 18:10:07
Report Time: 12.06.2018 11:43:27
Sample Mass: 0,4530 g
Cold Free Space: 31,7370 cm³
Low Pressure Dose: None
Automatic Degas: No

Analysis Adsorptive: N2
Analysis Bath Temp.: -195,800 °C
Thermal Correction: No
Warm Free Space: 11,0346 cm³ Measured
Equilibration Interval: 5 s
Sample Density: 1,000 g/cm³

Isotherm Tabular Report

Relative Pressure (p/p°)	Absolute Pressure (mmHg)	Quantity Adsorbed (mmol/g)	Elapsed Time (h:min)	Saturation Pressure (mmHg)
0.651539199	482.139008	1.77260	02:42	
0.601008606	444.746368	1.73889	02:45	
0.551930979	408.428925	1.70327	02:48	
0.505650041	374.181030	1.65072	02:53	
0.451777443	334.315308	1.42233	03:06	
0.404210271	299.115601	1.29208	03:13	
0.338776047	250.694275	1.18131	03:20	
0.296885124	219.694992	1.11617	03:24	
0.252854940	187.112656	1.05047	03:29	
0.202514834	149.860977	0.97729	03:33	
0.141622925	104.800964	0.88854	03:38	

Sample: template_180607
Operator: Kin
Submitter: Kin
File: C:\TriStar II 3020\d...\template_180607 - Cu_Port3.SMP

Started: 07.06.2018 14:30:30
Completed: 07.06.2018 18:10:07
Report Time: 12.06.2018 11:43:27
Sample Mass: 0,4530 g
Cold Free Space: 31,7370 cm³
Low Pressure Dose: None
Automatic Degas: No

Analysis Adsorptive: N2
Analysis Bath Temp.: -195,800 °C
Thermal Correction: No
Warm Free Space: 11,0346 cm³ Measured
Equilibration Interval: 5 s
Sample Density: 1,000 g/cm³

Isotherm Linear Plot

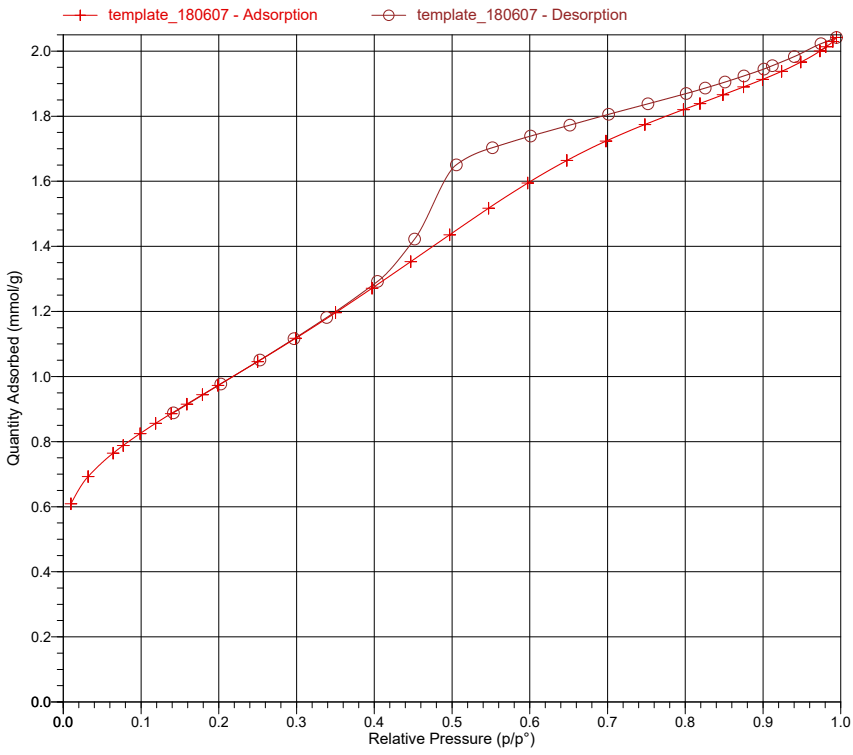

Sample: template_180607
Operator: Kin
Submitter: Kin
File: C:\TriStar II 3020\d...\template_180607 - Cu_Port3.SMP

Started:	07.06.2018 14:30:30	Analysis Adsorptive:	N2
Completed:	07.06.2018 18:10:07	Analysis Bath Temp.:	-195,800 °C
Report Time:	12.06.2018 11:43:27	Thermal Correction:	No
Sample Mass:	0,4530 g	Warm Free Space:	11,0346 cm³ Measured
Cold Free Space:	31,7370 cm³	Equilibration Interval:	5 s
Low Pressure Dose:	None	Sample Density:	1,000 g/cm³
Automatic Degas:	No		

BET Report

BET Surface Area: 77.8017 ± 0.4051 m²/g
Slope: 1.245731 ± 0.006388 g/mmol
Y-Intercept: 0.008215 ± 0.001350 g/mmol
C: 152.632023
Qm: 0,79748 mmol/g
Correlation Coefficient: 0.9999474
Molecular Cross-Sectional Area: 0.1620 nm²

Relative Pressure (p/p°)	Quantity Adsorbed (mmol/g)	1/[Q(p°/p - 1)]
0.138857960	0.88621	0.18195
0.158889430	0.91534	0.20638
0.178911116	0.94415	0.23079
0.199007189	0.97278	0.25540
0.250058684	1.04585	0.31882
0.298906275	1.11749	0.38152

Sample: template_180607
Operator: Kin
Submitter: Kin
File: C:\TriStar II 3020\d...\template_180607 - Cu_Port3.SMP

Started:	07.06.2018 14:30:30	Analysis Adsorptive:	N2
Completed:	07.06.2018 18:10:07	Analysis Bath Temp.:	-195,800 °C
Report Time:	12.06.2018 11:43:27	Thermal Correction:	No
Sample Mass:	0,4530 g	Warm Free Space:	11,0346 cm³ Measured
Cold Free Space:	31,7370 cm³	Equilibration Interval:	5 s
Low Pressure Dose:	None	Sample Density:	1,000 g/cm³
Automatic Degas:	No		

BET Surface Area Plot

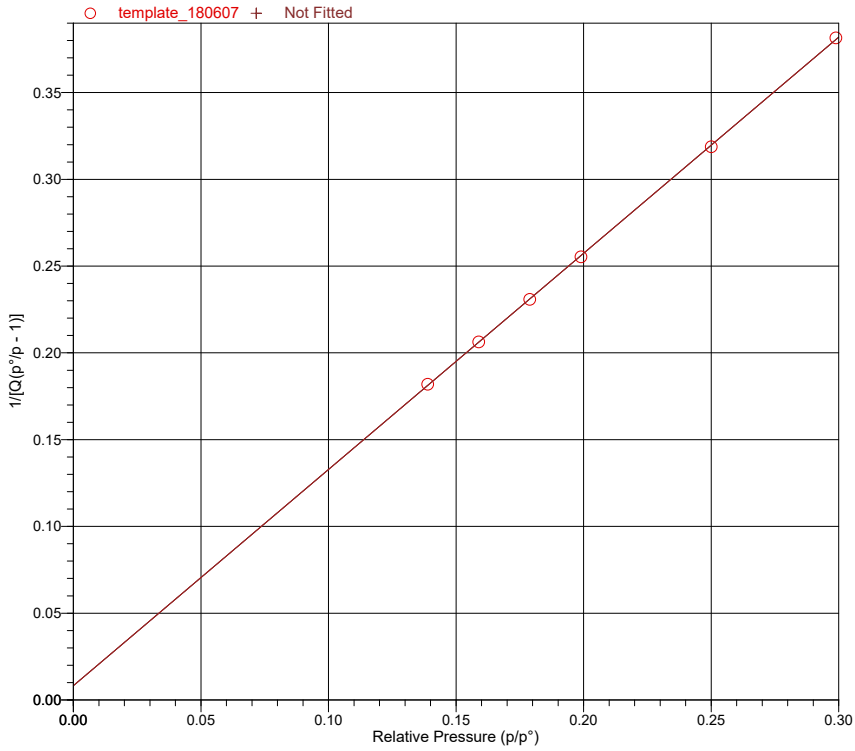

Sample: template_180607
Operator: Kin
Submitter: Kin
File: C:\TriStar II 3020\d...\template_180607 - Cu_Port3.SMP

Started: 07.06.2018 14:30:30
Completed: 07.06.2018 18:10:07
Report Time: 12.06.2018 11:43:27
Sample Mass: 0,4530 g
Cold Free Space: 31,7370 cm³
Low Pressure Dose: None
Automatic Degas: No

Analysis Adsorptive: N2
Analysis Bath Temp.: -195,800 °C
Thermal Correction: No
Warm Free Space: 11,0346 cm³ Measured
Equilibration Interval: 5 s
Sample Density: 1,000 g/cm³

BJH Desorption dV/dw Pore Volume

Halsey : Faas Correction

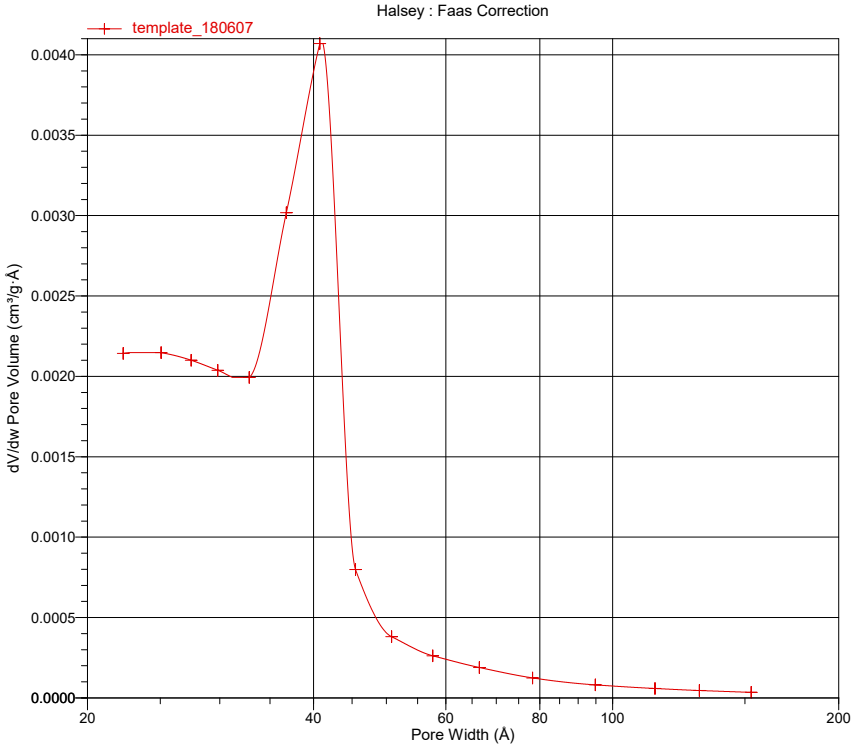

C.3 CZW-CuImpr

Full Report Set

Sample: template_180607
Operator: Kin
Submitter: Kin
File: C:\TriStar II 3020\...\template_180607 - CuI_Port1.SMP

Started: 07.06.2018 14:30:30
Completed: 07.06.2018 18:10:07
Report Time: 12.06.2018 11:42:51
Sample Mass: 0,2570 g
Cold Free Space: 33,6949 cm³
Low Pressure Dose: None
Automatic Degas: No

Analysis Adsorptive: N2
Analysis Bath Temp.: -195,800 °C
Thermal Correction: No
Warm Free Space: 11,5634 cm³ Measured
Equilibration Interval: 5 s
Sample Density: 1,000 g/cm³

Summary Report

Surface Area

Single point surface area at p/p° = 0,300126380: 40,6358 m²/g

BET Surface Area: 41,7296 m²/g

Pore Volume

Single point adsorption total pore volume of pores less than 11,415 Å width at p/p° = 0,010000000: 0,010966 cm³/g

BJH Adsorption cumulative volume of pores between 17,000 Å and 3 000,000 Å width: 0,067174 cm³/g

BJH Desorption cumulative volume of pores between 17,000 Å and 3 000,000 Å width: 0,080512 cm³/g

Pore Size

Adsorption average pore diameter (4V/A by BET): 10,5114 Å

BJH Adsorption average pore width (4V/A): 59,273 Å

BJH Desorption average pore width (4V/A): 62,411 Å

Freundlich

Qm·C: 0,00227 ± 0.0068 mmol/g

m: 1.9156 ± 0.2003

Temkin

q·alpha/Qm: 1.239879 ± 0.209166 kJ/mol·(mmol/g)

A: 0.0367 ± 0.0405 mmHg

Sample: template_180607
Operator: Kin
Submitter: Kin
File: C:\TriStar II 3020\...\template_180607 - CuI_Port1.SMP

Started: 07.06.2018 14:30:30
Completed: 07.06.2018 18:10:07
Report Time: 12.06.2018 11:42:51
Sample Mass: 0,2570 g
Cold Free Space: 33,6949 cm³
Low Pressure Dose: None
Automatic Degas: No

Analysis Adsorptive: N2
Analysis Bath Temp.: -195,800 °C
Thermal Correction: No
Warm Free Space: 11,5634 cm³ Measured
Equilibration Interval: 5 s
Sample Density: 1,000 g/cm³

Isotherm Tabular Report

Relative Pressure (p/p°)	Absolute Pressure (mmHg)	Quantity Adsorbed (mmol/g)	Elapsed Time (h:min)	Saturation Pressure (mmHg)
				740.000000
0.009617492	7.116944	0.31467	00:29	
0.029347177	21.716911	0.35601	00:31	
0.063727064	47.158028	0.39739	00:33	
0.078917524	58.398968	0.41221	00:35	
0.099600395	73.704292	0.43110	00:37	
0.120218143	88.961426	0.44886	00:38	
0.140128955	103.695427	0.46559	00:40	
0.160059326	118.443901	0.48192	00:41	
0.180522836	133.586899	0.49831	00:43	
0.200147618	148.109238	0.51410	00:44	
0.248114302	183.604584	0.55267	00:46	
0.300126380	222.093521	0.59514	00:48	
0.350127885	259.094635	0.63814	00:49	
0.399324613	295.500214	0.68266	00:51	
0.449034778	332.285736	0.73135	00:53	
0.498973826	369.240631	0.78508	00:55	
0.548713272	406.047821	0.84499	00:57	
0.598313409	442.751923	0.91416	01:00	
0.647937754	479.473938	0.99630	01:02	
0.697387860	516.067017	1.09548	01:05	
0.746271742	552.241089	1.21980	01:09	
0.794972435	588.279602	1.38291	01:13	
0.819243972	606.240540	1.48342	01:16	
0.846497572	626.408203	1.62254	01:21	
0.871979667	645.264954	1.77390	01:25	
0.895937451	662.993713	1.94369	01:30	
0.921225141	681.706604	2.14868	01:36	
0.946028756	700.061279	2.37190	01:42	
0.971435794	718.862488	2.61020	01:47	
0.978856762	724.354004	2.68418	01:51	
0.989038416	731.888428	2.77913	01:55	
0.993494477	735.185913	2.82518	01:58	
0.976070095	722.291870	2.78020	02:00	
0.962525816	712.269104	2.72720	02:02	
0.943088098	697.885193	2.63914	02:05	
0.926768205	685.808472	2.55634	02:08	
0.903898084	668.884583	2.42928	02:12	
0.878583753	650.151978	2.27303	02:17	
0.853043840	631.252441	2.10619	02:22	
0.827873766	612.626587	1.94089	02:27	
0.803231482	594.391296	1.78072	02:32	
0.748019409	553.534363	1.47851	02:40	

Sample: template_180607
Operator: Kin
Submitter: Kin
File: C:\TriStar II 3020\...\template_180607 - CuI_Port1.SMP

Started: 07.06.2018 14:30:30
Completed: 07.06.2018 18:10:07
Report Time: 12.06.2018 11:42:51
Sample Mass: 0,2570 g
Cold Free Space: 33,6949 cm³
Low Pressure Dose: None
Automatic Degas: No

Analysis Adsorptive: N2
Analysis Bath Temp.: -195,800 °C
Thermal Correction: No
Warm Free Space: 11,5634 cm³ Measured
Equilibration Interval: 5 s
Sample Density: 1,000 g/cm³

Isotherm Tabular Report

Relative Pressure (p/p°)	Absolute Pressure (mmHg)	Quantity Adsorbed (mmol/g)	Elapsed Time (h:min)	Saturation Pressure (mmHg)
0.704524190	521.347900	1.28999	02:46	
0.654447566	484.291199	1.12395	02:50	
0.603805377	446.815979	0.99798	02:54	
0.553257174	409.410309	0.90208	02:57	
0.502674082	371.978821	0.82473	02:59	
0.454504271	336.333160	0.74310	03:02	
0.401150966	296.851715	0.68237	03:04	
0.352646286	260.958252	0.63713	03:06	
0.301324917	222.980438	0.59274	03:08	
0.250740732	185.548141	0.55074	03:10	
0.200483209	148.357574	0.51002	03:12	
0.140872564	104.245697	0.46142	03:14	

Sample: template_180607
Operator: Kin
Submitter: Kin
File: C:\TriStar II 3020\...\template_180607 - CuI_Port1.SMP

Started:	07.06.2018 14:30:30	Analysis Adsorptive:	N2
Completed:	07.06.2018 18:10:07	Analysis Bath Temp.:	-195,800 °C
Report Time:	12.06.2018 11:42:51	Thermal Correction:	No
Sample Mass:	0,2570 g	Warm Free Space:	11,5634 cm³ Measured
Cold Free Space:	33,6949 cm³	Equilibration Interval:	5 s
Low Pressure Dose:	None	Sample Density:	1,000 g/cm³
Automatic Degas:	No		

Isotherm Linear Plot

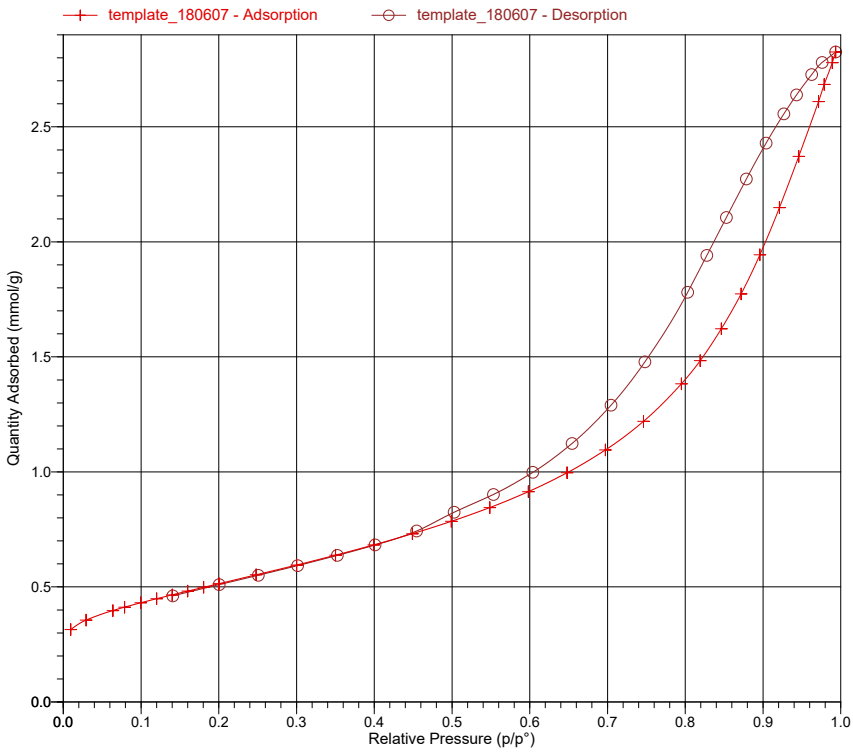

Sample: template_180607
Operator: Kin
Submitter: Kin
File: C:\TriStar II 3020\...\template_180607 - CuI_Port1.SMP

Started: 07.06.2018 14:30:30
Completed: 07.06.2018 18:10:07
Report Time: 12.06.2018 11:42:51
Sample Mass: 0,2570 g
Cold Free Space: 33,6949 cm³
Low Pressure Dose: None
Automatic Degas: No

Analysis Adsorptive: N2
Analysis Bath Temp.: -195,800 °C
Thermal Correction: No
Warm Free Space: 11,5634 cm³ Measured
Equilibration Interval: 5 s
Sample Density: 1,000 g/cm³

BET Report

BET Surface Area: 41.7296 ± 0.1869 m²/g
Slope: 2.313073 ± 0.010242 g/mmol
Y-Intercept: 0.024812 ± 0.002171 g/mmol
C: 94.222936
Qm: 0,42774 mmol/g
Correlation Coefficient: 0.9999608
Molecular Cross-Sectional Area: 0.1620 nm²

Relative Pressure (p/p°)	Quantity Adsorbed (mmol/g)	1/[Q(p°/p - 1)]
0.140128955	0.46559	0.35002
0.160059326	0.48192	0.39542
0.180522836	0.49831	0.44208
0.200147618	0.51410	0.48673
0.248114302	0.55267	0.59708
0.300126380	0.59514	0.72055

Sample: template_180607
Operator: Kin
Submitter: Kin
File: C:\TriStar II 3020\...\template_180607 - CuI_Port1.SMP

Started:	07.06.2018 14:30:30	Analysis Adsorptive:	N2
Completed:	07.06.2018 18:10:07	Analysis Bath Temp.:	-195,800 °C
Report Time:	12.06.2018 11:42:51	Thermal Correction:	No
Sample Mass:	0,2570 g	Warm Free Space:	11,5634 cm³ Measured
Cold Free Space:	33,6949 cm³	Equilibration Interval:	5 s
Low Pressure Dose:	None	Sample Density:	1,000 g/cm³
Automatic Degas:	No		

BET Surface Area Plot

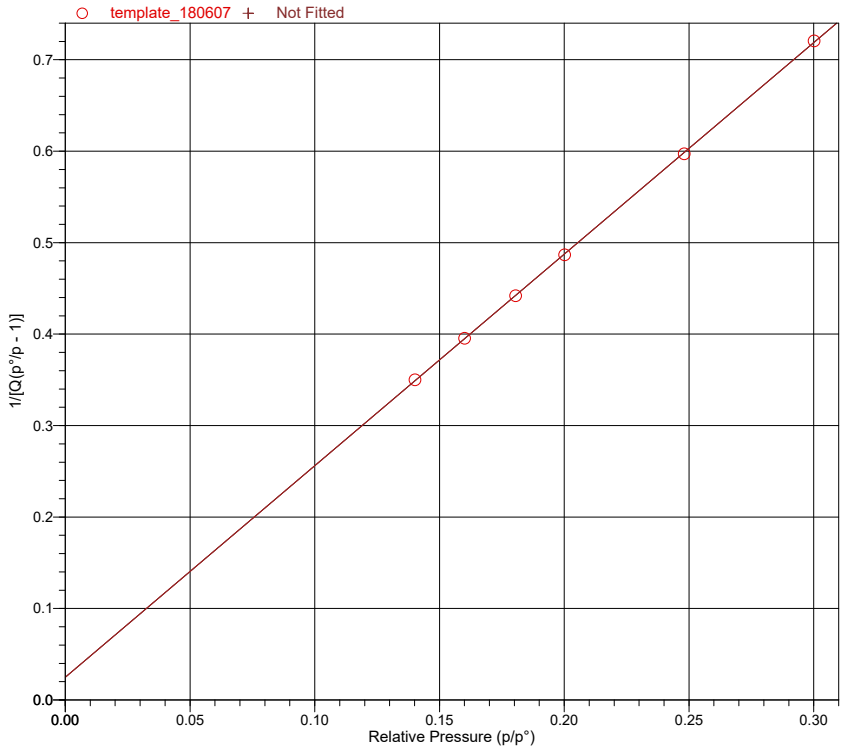

Sample: template_180607
Operator: Kin
Submitter: Kin
File: C:\TriStar II 3020\...\template_180607 - CuI_Port1.SMP

Started:	07.06.2018 14:30:30	Analysis Adsorptive:	N2
Completed:	07.06.2018 18:10:07	Analysis Bath Temp.:	-195,800 °C
Report Time:	12.06.2018 11:42:51	Thermal Correction:	No
Sample Mass:	0,2570 g	Warm Free Space:	11,5634 cm³ Measured
Cold Free Space:	33,6949 cm³	Equilibration Interval:	5 s
Low Pressure Dose:	None	Sample Density:	1,000 g/cm³
Automatic Degas:	No		

BJH Desorption dV/dw Pore Volume

Halsey : Faas Correction

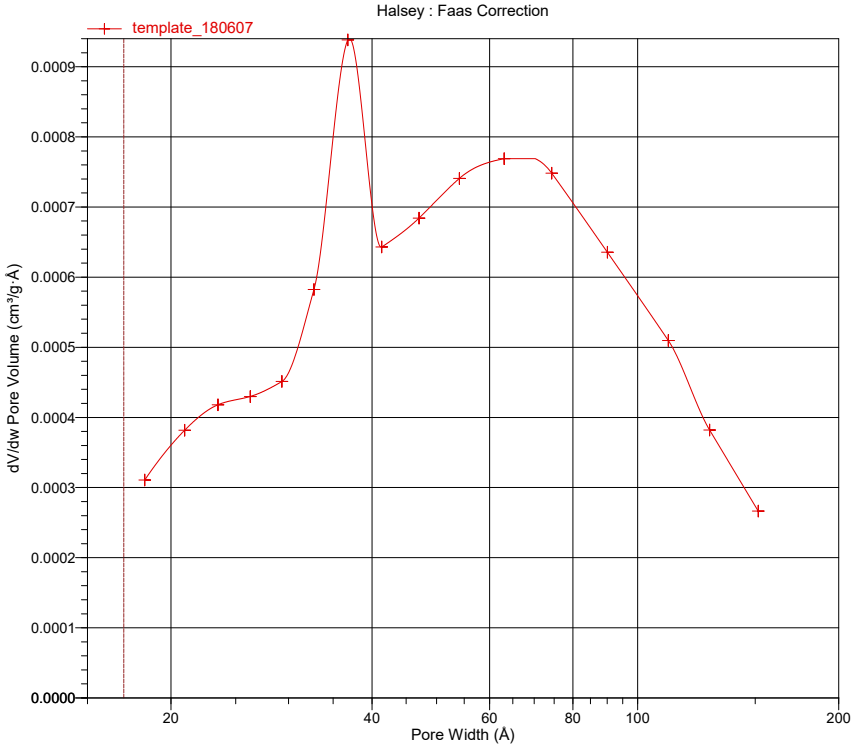

Appendix D

Activity plot

D.1 CZW

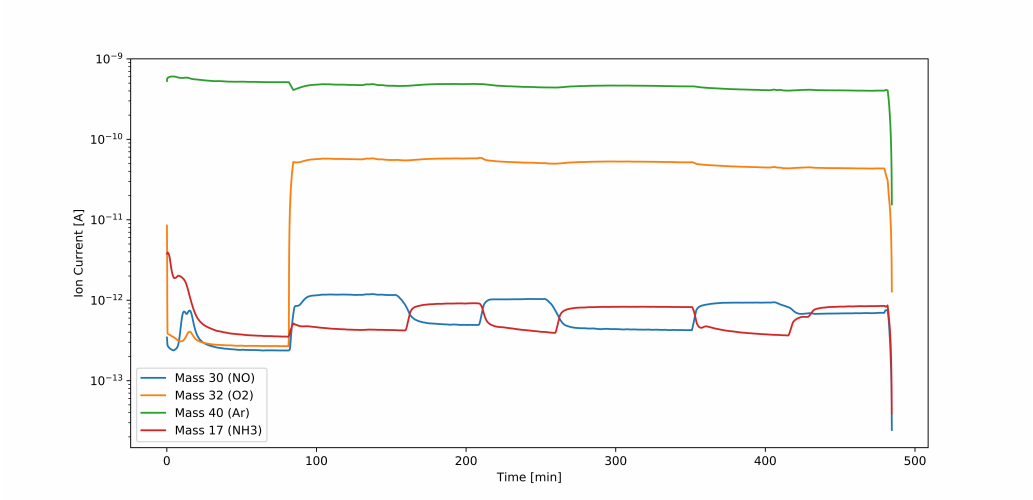

D.2 CZW-Cu

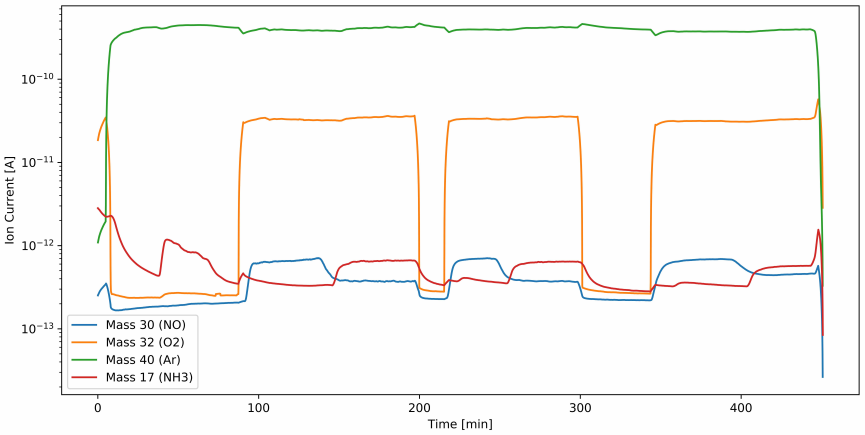

D.3 CZW-CuImpr

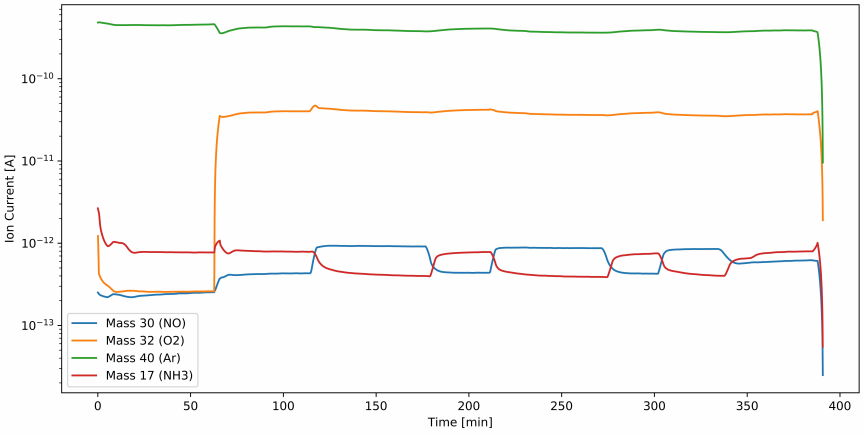

Appendix E

Risk analysis

ID	27118	**Status**	**Dato**
Risikoområde	Risikovurdering: Helse, miljø og sikkerhet (HMS)	Opprettet	09.02.2018
Opprettet av	Kin Hui	Vurdering startet	09.02.2018
Ansvarlig	Kin Hui	Tiltak besluttet	
		Avsluttet	

Risikovurdering:

CAT, Master student, 2017, Chun Kin Hui

Gyldig i perioden:
2/9/2018 - 7/1/2018

Sted:
Trondheim

Mål / hensikt
Synthesize a new catalyst to reduce NOx formation in marine propulsion systems.
Test the catalyst in a capillary reactor in rigg 2.8

Bakgrunn
Making a new low temperature selective catalytic reduction catalyst, as a part of my master project.

Beskrivelse og avgrensninger
By using Zirconium, Cerium and Tungsten oxide by hydrothermal method. Stirring in glycerol bath at medium temperatures. Stored in an autoclave for 3 days, dried and calcined. run through several characterization equipments to determine the catalyst properties.

Sample preparation for the activity measurements.

Forutsetninger, antakelser og forenklinger
[Ingen registreringer]

Vedlegg
[Ingen registreringer]

Referanser
[Ingen registreringer]

Oppsummering, resultat og endelig vurdering

I oppsummeringen presenteres en oversikt over farer og uønskede hendelser, samt resultat for det enkelte konsekvensområdet.

Farekilde:	**Use of furnace**		
Uønsket hendelse:	**Burn**		
Konsekvensområde:	Helse	Risiko før tiltak:	Risiko etter tiltak:

Farekilde:	**spilling of chemicals (Acid)**		
Uønsket hendelse:	**acid burn**		
Konsekvensområde:	Helse	Risiko før tiltak:	Risiko etter tiltak:
	Materielle verdier	Risiko før tiltak:	Risiko etter tiltak:

Farekilde:	**Catalyst preparation**		
Uønsket hendelse:	**Formation of harmful chemicals/gases**		
Konsekvensområde:	Helse	Risiko før tiltak:	Risiko etter tiltak:
	Ytre miljø	Risiko før tiltak:	Risiko etter tiltak:

Farekilde:	**Gas leakage**		
Uønsket hendelse:	**Exposure to NO, NO2**		
Konsekvensområde:	Helse	Risiko før tiltak:	Risiko etter tiltak:

Endelig vurdering

General lab with no special chemicals is involved, should be perfectly fine doing this alone even outside of office hours.

Involverte enheter og personer

En risikovurdering kan gjelde for en, eller flere enheter i organisasjonen. Denne oversikten presenterer involverte enheter og personell for gjeldende risikovurdering.

Enhet /-er risikovurderingen omfatter

- NTNU

Deltakere

[Ingen registreringer]

Lesere

Magnus Rønning
Ole Håvik Bjørkedal
Karin Wiggen Dragsten
Edd Anders Blekkan

Andre involverte/interessenter

[Ingen registreringer]

Følgende akseptkriterier er besluttet for risikoområdet Risikovurdering: Helse, miljø og sikkerhet (HMS):

Helse

Materielle verdier

Omdømme

Ytre miljø

Oversikt over eksisterende, relevante tiltak som er hensyntatt i risikovurderingen

I tabellen under presenteres eksisterende tiltak som er hensyntatt ved vurdering av sannsynlighet og konsekvens for aktuelle uønskede hendelser.

Farekilde	Uønsket hendelse	Tiltak hensyntatt ved vurdering
Use of furnace	Burn	
spilling of chemicals (Acid)	acid burn	Personal safety equipments
Catalyst preparation	Formation of harmful chemicals/gases	Fume hood
Gas leakage	Exposure to NO, NO2	Gas detector

Eksisterende og relevante tiltak med beskrivelse:

Personal safety equipments
Goggles, lab coat

Fume hood
[Ingen registreringer]

Gas detector
[Ingen registreringer]

Risikoanalyse med vurdering av sannsynlighet og konsekvens

I denne delen av rapporten presenteres detaljer dokumentasjon av de farer, uønskede hendelser og årsaker som er vurdert. Innledningsvis oppsummeres farer med tilhørende uønskede hendelser som er tatt med i vurderingen.

Følgende farer og uønskede hendelser er vurdert i denne risikovurderingen:

- **Use of furnace**
  - Burn
- **spilling of chemicals (Acid)**
  - acid burn
- **Catalyst preparation**
  - Formation of harmful chemicals/gases
- **Gas leakage**
  - Exposure to NO, NO2

Detaljert oversikt over farekilder og uønskede hendelser:

Farekilde: Use of furnace

use of furnace for calcination or just drying of sample and equipments

Uønsket hendelse: Burn

Sannsynlighet for hendelsen (felles for alle konsekvensområder): **Sannsynlig (3)**

Kommentar:
Accidents can happen

Konsekvensområde: Helse

Risiko:

Vurdert konsekvens: **Liten (1)**

Kommentar: [Ingen registreringer]

Farekilde: spilling of chemicals (Acid)

Uønsket hendelse: acid burn

Årsak: accident

Sannsynlighet for hendelsen (felles for alle konsekvensområder): **Lite sannsynlig (2)**

Kommentar:
[Ingen registreringer]

Konsekvensområde: Helse

Vurdert konsekvens: **Middels (2)**

Kommentar: [Ingen registreringer]

Risiko:

Konsekvensområde: Materielle verdier

Vurdert konsekvens: **Middels (2)**

Kommentar: [Ingen registreringer]

Risiko:

Farekilde: Catalyst preparation

Synthesizing of new catalyst

Uønsket hendelse: Formation of harmful chemicals/gases

Sannsynlighet for hendelsen (felles for alle konsekvensområder): **Lite sannsynlig (2)**

Kommentar:
[Ingen registreringer]

Konsekvensområde: Helse

Risiko:

Vurdert konsekvens: **Middels (2)**

Kommentar: [Ingen registreringer]

Konsekvensområde: Ytre miljø

Risiko:

Vurdert konsekvens: **Middels (2)**

Kommentar: [Ingen registreringer]

Farekilde: Gas leakage

Uønsket hendelse: Exposure to NO, NO2

Sannsynlighet for hendelsen (felles for alle konsekvensområder): **Svært lite sannsynlig (1)**

Kommentar:
[Ingen registreringer]

Konsekvensområde: Helse

Risiko:

Vurdert konsekvens: **Stor (3)**

Kommentar: [Ingen registreringer]

Oversikt over besluttede risikoreduserende tiltak:

Under presenteres en oversikt over risikoreduserende tiltak som skal bidra til å reduseres sannsynlighet og/eller konsekvens for uønskede hendelser.

Detaljert oversikt over besluttede risikoreduserende tiltak med beskrivelse:

Detaljert oversikt over vurdert risiko for hver farekilde/uønsket hendelse før og etter besluttede tiltak